



Deposited via The University of Sheffield.

White Rose Research Online URL for this paper:

<https://eprints.whiterose.ac.uk/id/eprint/89310/>

Version: Accepted Version

Article:

Schuch, B., Feigenbutz, M., Makino, D.L. et al. (2014) The exosome-binding factors Rrp6 and Rrp47 form a composite surface for recruiting the Mtr4 helicase. *EMBO Journal*, 33 (23). 2829 - 2846. ISSN: 0261-4189

<https://doi.org/10.15252/emj.201488757>

Reuse

Items deposited in White Rose Research Online are protected by copyright, with all rights reserved unless indicated otherwise. They may be downloaded and/or printed for private study, or other acts as permitted by national copyright laws. The publisher or other rights holders may allow further reproduction and re-use of the full text version. This is indicated by the licence information on the White Rose Research Online record for the item.

Takedown

If you consider content in White Rose Research Online to be in breach of UK law, please notify us by emailing eprints@whiterose.ac.uk including the URL of the record and the reason for the withdrawal request.

**The exosome-binding factors Rrp6 and Rrp47
form a composite surface for recruiting the Mtr4 helicase**

Benjamin Schuch¹, Monika Feigenbutz², Debora L. Makino¹, Sebastian Falk¹, Claire Basquin¹, Phil Mitchell² and Elena Conti¹

¹ Structural Cell Biology Department, Max Planck Institute of Biochemistry, Am Klopferspitz 18, D-82152 Martinsried, Germany

² Molecular Biology and Biotechnology Department, The University of Sheffield, Sheffield S10 2TN, UK.

Running title: Structure of the Rrp6-Rrp47-Mtr4 interaction

Abstract

The exosome is a conserved multi-subunit ribonuclease complex that functions in 3' end processing, turnover and surveillance of nuclear and cytoplasmic RNAs. In the yeast nucleus, the 10-subunit core complex of the exosome (Exo-10) physically and functionally interacts with the Rrp6 exoribonuclease and its associated cofactor Rrp47, the helicase Mtr4 and the exosome cofactor Mpp6. Here we show that binding of Mtr4 to Exo-10 in vitro is dependent upon both Rrp6 and Rrp47, whereas Mpp6 binds directly and independently of other cofactors. Crystallographic analyses reveal that the N-terminal domains of Rrp6 and Rrp47 form a highly intertwined structural unit. Rrp6 and Rrp47 synergize to create a composite and conserved surface groove that binds the N-terminus of Mtr4. Mutation of conserved residues within Rrp6 and Mtr4 at the structural interface disrupt their interaction and inhibit growth of strains expressing a C-terminal GFP fusion of Mtr4. These studies provide detailed structural insight into the interaction between the Rrp6 - Rrp47 complex and Mtr4 that mediates an important link between Mtr4 and the core exosome.

Introduction

Most cellular ribonucleic acids are transcribed in the nucleus as larger precursor molecules that are then processed to produce mature, functional RNAs. The maturation of ribosomal RNAs (rRNAs), small nuclear and nucleolar RNAs (snRNAs and snoRNAs) requires the trimming of the extended 3' end of their nascent transcripts and the elimination of the excised RNA fragments (reviewed in Bernstein & Toth, 2012). These processes involve a complex of ribonucleases known as the RNA exosome (Allmang *et al*, 1999a). In addition to 3' end processing, the exosome functions in RNA turnover and surveillance pathways (reviewed in Schmid & Jensen, 2008; Schaeffer *et al*, 2011; Chlebowski *et al*, 2013). In the nucleus, it mediates the turnover of precursor transfer RNAs (pre-tRNAs) and precursor messenger RNAs (pre-mRNAs) (Gudipati *et al*, 2012). The nuclear exosome also swiftly eliminates misprocessed tRNAs (Kadaba *et al*, 2004) and pre-mRNAs (Bousquet-Antonelli *et al*, 2000; Hilleren *et al*, 2001) as well as cryptic unstable transcripts (CUTs) generated by antisense and intergenic transcription (Wyers *et al*, 2005; Davis & Ares, 2006; Neil *et al*, 2009). In the cytoplasm, the exosome participates in the turnover of mature mRNAs (Anderson & Parker, 1998) and in quality-control pathways that eliminate defective mRNAs with premature stop codons (Mitchell & Tollervey, 2003) or without a stop codon (van Hoof *et al*, 2002).

The exosome core complex consists of ten subunits that are evolutionarily conserved and are essential in yeast (Allmang *et al*, 1999b). Nine of these subunits form a catalytically inactive barrel-like structure (Exo-9) (Liu *et al*, 2006; Dziembowski *et al*, 2007) that threads RNA substrates to the tenth subunit, Rrp44 (also known as Dis3) (Bonneau *et al*, 2009; Malet *et al*, 2010; Wasmuth & Lima, 2012; Makino *et al*, 2013a; Liu *et al*, 2014). Rrp44 is bound at the bottom of the Exo-

9 barrel and contains a processive 3'-5'-exoribonuclease site and an endonuclease site (reviewed in Schneider & Tollervey, 2013; Makino *et al*, 2013b). While the Exo-10 core is found in both the nucleus and the cytoplasm, physical and genetic interactions have linked the exosome core to several cofactors that have specific subcellular localization (reviewed in Schneider & Tollervey, 2013). In the cytoplasm, the exosome functions together with the Ski complex, a multi-subunit assembly centered at the helicase Ski2 (Anderson & Parker, 1998; Araki *et al*, 2001; Halbach *et al*, 2013). In the yeast nucleus, the exosome is associated with a set of conserved proteins that include Rrp6 (known as PM/ScI-100 in humans), Rrp47 (also known as Lrp1 in yeast and as C1D in humans), Mpp6 and Mtr4 (also known as Dob1 in yeast) (reviewed in Butler & Mitchell, 2011).

Rrp6 contains a 3'-5'-exoribonuclease site. In contrast to Rrp44, the Rrp6 nuclease functions in a distributive manner and stalls when encountering structured RNA sequences (Briggs *et al*, 1998; Burkard & Butler, 2000; Liu *et al*, 2006; Januszyk *et al*, 2011). Rrp6 binds the exosome directly, near the top of the Exo-9 barrel (Cristodero *et al*, 2008; Makino *et al*, 2013a; Wasmuth *et al*, 2014). Although *in vitro* Rrp6 and Rrp44 can bind Exo-9 independently of each other, Exo-9 binding interconnects the enzymatic properties of the two ribonucleases (Liu *et al*, 2006; Wasmuth & Lima, 2012). The interplay between Rrp6 and Rrp44 also emerges from *in vivo* studies. During the maturation of 5.8S rRNA, Rrp44 degrades the 3' end of the precursor to leave a processing intermediate that is then trimmed to the final product by Rrp6. This intermediate features a 3' extension of 30 nucleotides (Briggs *et al*, 1998), a length that corresponds to the size of the internal channel of Exo-10 (Bonneau *et al*, 2009; Makino *et al*, 2013a). Rrp6 can carry out the last processing step even when separated from Exo-10 (Callahan & Butler, 2008).

Rrp47 and Rrp6 interact *in vitro* (Stead *et al*, 2007) and *in vivo* (Mitchell *et al*, 2003; Synowsky *et al*, 2009). Consistently, depletion of Rrp47 leads to defects in RNA processing and degradation that are similar to those observed in *rrp6Δ* strains (Mitchell *et al*, 2003; Peng *et al*, 2003). The presence of Rrp6 protects Rrp47 from degradation in yeast and conversely Rrp47 stabilizes Rrp6 (Stuparevic *et al*, 2013; Feigenbutz *et al*, 2013b; 2013a). Knockout of either Rrp6 or Rrp47 is synthetically lethal with the absence of Mpp6, another factor that functions in the maturation of 5.8S rRNA, the degradation of CUTs and pre-mRNA surveillance (Milligan *et al*, 2008). The human orthologue of Mpp6 has been shown to interact with PM-Scl100 – C1D (Rrp6 – Rrp47) in co-immunoprecipitation experiments, and also with human Mtr4 (Schilders *et al*, 2007). Mtr4 is a Ski2-related RNA helicase (Jackson *et al*, 2010; Weir *et al*, 2010; Halbach *et al*, 2012) and is essential for viability in yeast (la Cruz *et al*, 1998). Mtr4 is required for Rrp6-dependent and Rrp6-independent functions of the nuclear exosome (Jackson *et al*, 2010; Klauer & van Hoof, 2013) and is also part of the TRAMP complex (LaCava *et al*, 2005; Wyers *et al*, 2005; Vanacova *et al*, 2005). In human cells, Mtr4 has been shown to associate with either Mpp6 (Schilders *et al*, 2007) or Rrp6 (Lubas *et al*, 2011). In yeast, all genetic data suggest a close association between Mtr4 and the exosome but no direct interaction has been reported thus far. In this work, we dissected the interaction network of the nuclear cofactors of the yeast exosome *in vitro* and identified the structural basis for how Rrp6 and Rrp47 assemble in a complex that directly recruits Mtr4.

Results

***S. cerevisiae* Rrp6 – Rrp47 recruits Mtr4 to the exosome**

The domain organization of nuclear cofactors of the *S. cerevisiae* exosome is in several cases known from previous structural studies or can be extrapolated from sequence analysis (Fig 1A). The Rrp6 exoribonuclease is a modular protein of 733 residues. The Rrp6 N-terminal region (so-called PMC2NT) mediates the interaction with Rrp47 and is expected to be a folded domain (Stead *et al*, 2007). The central region encompasses the exoribonuclease (Exo domain), which includes the catalytic DEDD site and the regulatory HRDC domain (Midtgaard *et al*, 2006). The C-terminal region consists of mainly low-complexity sequences and contains both the Exo-9-binding segment and two nuclear localization signals (NLSs) (Callahan & Butler, 2008; Makino *et al*, 2013a). Rrp47 (184 residues) has an N-terminal domain that binds Rrp6 and a C-terminal low-complexity region rich in positively charged residues (Costello *et al*, 2011) (Fig 1A). The Mtr4 helicase (1073 residues) contains a low-complexity N-terminal region of 80 residues followed by a DExH helicase core characterized by an insertion domain also known as the arch domain (Weir *et al*, 2010; Jackson *et al*, 2010) (Fig 1A). Mpp6 (186 residues) is a small basic protein without recognizable domains.

We recombinantly expressed and purified different versions of these proteins, incubated them in different combinations and analyzed the mixtures using size-exclusion chromatography to dissect their direct interactions (Fig 1B-1G). In the case of Rrp6, we engineered a version of the protein that spans from the Rrp47-binding domain to the exosome-binding domain (Rrp6_{ΔNLS}), as the inclusion of the very C-terminus resulted in an unstable sample that was quickly degraded. Rrp6_{ΔNLS} co-

eluted with full-length Rrp47 (Fig 1B, peak 1 in the size exclusion chromatography profile on the left and lane 1 in the corresponding Coomassie gel on the right). Rrp6 Δ NLS – Rrp47 did not interact with Mpp6 (Fig 1B, peaks and lanes 2 and 3). Instead, Rrp6 Δ NLS – Rrp47 interacted with full-length Mtr4 (Fig 1B, peak and lane 2). Interestingly, Mtr4 required the Rrp6 Δ NLS – Rrp47 complex to bind to Exo-9 (Fig 1C, compare peak and lane 1, with peaks and lanes 4 and 5). Rrp6 lacking the N-terminal Rrp47-binding domain (Rrp6 Δ N) co-eluted with Exo-9 but lost most of the binding to Mtr4 (Fig 1C, peaks and lanes 5 and 6). The other nuclear exosome cofactor, Mpp6, interacted with Exo-9 both in the presence and in the absence of Rrp6 Δ NLS – Rrp47 (Fig 1D, peak and lane 1, compare with peak and lane 2). Finally, Exo-9, Rrp6 Δ NLS, Rrp47, Mtr4, Mpp6 and Rrp44 co-eluted in a single peak that corresponds to the 14-subunit nuclear exosome (Fig 1D, peak and lane 6). These data indicate that *S. cerevisiae* Rrp6, Rrp44 and Mpp6 can bind directly, independently and concomitantly to Exo-9, while Mtr4 is recruited to the exosome mainly by binding to Rrp6 – Rrp47.

The N-terminal domains of Mtr4, Rrp6 and Rrp47 form a ternary complex *in vitro*

Consistent with previous studies (Stead *et al*, 2007; Costello *et al*, 2011; Dedic *et al*, 2014), we observed an interaction between the N-terminal regions of Rrp6 (Rrp6 Δ N, residues 1-111) and Rrp47 (Rrp47 Δ C, residues 1-133) (Fig. 1A). Rrp6 Δ N and Rrp47 Δ C co-eluted with Mtr4 in size-exclusion assays (Fig 1E, peak and lane 1). Next, we assessed which part of Mtr4 is recognized by Rrp6 – Rrp47. Rrp6 Δ N and Rrp47 Δ C co-eluted with the N-terminal region of Mtr4 (Mtr4 Δ 80) (Fig 1F, lane and peak 1), while no interaction was detected with the helicase domain (Mtr4 Δ 80) (Fig 1E, peaks and lanes

4 and 5). In isolation, neither Rrp6_N nor Rrp47_{ΔC} interacted with Mtr4 (Fig 1G, peaks and lanes 1, 2 and 3, 4, respectively), suggesting that both proteins are required for binding. Finally, the interaction is conserved across species, as the *S. cerevisiae* Rrp6_N – Rrp47_{ΔC} complex formed a complex with the *N. crassa* Mtr4 orthologue, FRH (Fig E1A). Sequence analysis showed that only the first 20 residues of the N-terminal region of Mtr4 are evolutionarily conserved (Fig 4C). Rrp6_N – Rrp47_{ΔC} indeed formed a ternary complex with an Mtr4₁₋₂₀ peptide (Mtr4_N) (Fig E1B). As a note, the cytoplasmic Ski2 helicase does not contain an analogous N-terminal sequence, and consistently the cytoplasmic exosome complex does not contain Rrp6 and Rrp47. Finally, using limited proteolysis experiments we could narrow down the Rrp6-binding domain of Rrp47 even further to residues 1-103 (Rrp47_N) (Fig E1C and Fig 1A).

Structure determination of the Rrp6_N - Rrp47_N - Mtr4_N complex

Alone, Rrp47_{ΔC} eluted as an apparent oligomer in size exclusion chromatography (Fig 1G, peak 4), consistent with previous reports of its oligomeric nature when in isolation (Feigenbutz *et al*, 2013b). Upon co-expression, however, the Rrp6_N – Rrp47_{ΔC} complex eluted with a predominant peak corresponding to the expected molecular weight of a 1:1 complex (Fig 1G, peak 5). Rrp6_N – Rrp47_{ΔC} crystallized in a tetragonal space group with three independent binary complexes in the asymmetric unit (Fig E2A). The structure was determined by combining phases from single-wavelength anomalous dispersion (SAD) experiments using crystals containing tantalum bromide and crystals of selenomethionine-substituted protein. The model has been refined to 2.64 Å resolution with an *R*_{free} of 23.8%, *R*factor of 20.7% and good stereochemistry (Table I).

Based on the atomic model of the binary Rrp6_N – Rrp47_{ΔC} complex (Fig 2A) and on the limited proteolysis experiments (Fig E1C), we trimmed the C-terminus of Rrp47 further and crystallized a ternary complex of Rrp6_N, Rrp47_N and Mtr4_N. Rrp6_N – Rrp47_N – Mtr4_N crystallized in a merohedrally-twinned trigonal space group with three independent copies of the complex in the asymmetric unit (Fig E2B). The structure was determined by molecular replacement using the coordinates of Rrp6_N – Rrp47_{ΔC} in combination with anomalous dispersion from yttrium ions that were required for crystallization and mediated lattice contacts. The model has been refined to 2.4 Å resolution with an *R*_{free} of 23.9%, *R*factor of 19.4% and good geometry (Table I). The atomic models of Rrp6 and Rrp47 are very similar in the three ternary complexes in the asymmetric unit, and are also very similar when compared to the structure of the binary complex (root mean square deviation rmsd of 1.26 Å over 182 α -carbon atoms). The main difference is that in one of the three copies of Rrp6_N – Rrp47_{ΔC}, twenty more residues of the C-terminal helix of Rrp47 are well ordered as a result of lattice contacts with a symmetry related molecule (compare Fig 2A and Fig 2B, left panel). The atomic model of Mtr4 shows well-defined electron density from residue 4 up to residue 17 (Fig 2B and Fig E2C).

The Rrp6 – Rrp47 interaction: an intertwined structure

The Rrp6_N – Rrp47_N complex has a compact α -helical fold (Fig 2B). At the secondary structure level, Rrp6_N and Rrp47_N are remarkably similar. They both consist of three long α -helices (α 1, α 2 and α 3) with a short α -helix (α _{short}) between α 1 and α 2. The stretch of Rrp6_N encompassing the first helix-turn-helix (α 1– α _{short}– α 2) can be superposed to the equivalent stretch of Rrp47_N (rmsd of 2.06Å over 39 C α atoms) (Fig 2C). The main topological difference between the two proteins is that helix α 3 is

oriented antiparallel to $\alpha 2$ in the case of Rrp47_N, while it points in the opposite direction in the case of Rrp6_N (Fig 2C and topology in Fig 2D).

The secondary structure elements of Rrp6_N and Rrp47_N are highly intertwined (Fig 2B and 2D). The first helix-turn-helix of Rrp6_N interdigitates with the first helix-turn-helix of Rrp47_N, forming a heterodimeric 4-helix bundle (Fig 2D and 3A). The $\alpha 3$ helices of Rrp6_N and Rrp47_N pack against the side of the bundle that is lined by the $\alpha 2$ helices (Fig 2D and 3B). Evolutionarily conserved residues of the $\alpha 1$ and $\alpha 2$ helices form an extensive hydrophobic core in the center of the bundle (Fig 3A, 4A and 4B). The interactions between the $\alpha 2$ and $\alpha 3$ helices are also extensive, apolar and conserved (Fig 3B, 4A and 4B). The interaction of Rrp6_N with Rrp47_N buries 5460 Å² (i.e. more than 33%) of the surface area of the two proteins. The complex appears to be further stabilized by inter-molecular salt-bridges present on the outer surface of the heterodimer. Finally, the structure of the binary complex shows that the C-terminal helix of Rrp47 protrudes out of the globular core of Rrp6_N – Rrp47_{ΔC}, extending about 30 Å into the solvent (Fig 2A). The C-terminal region of Rrp47 that has been reported to interact with proteins involved in snoRNP assembly (Costello *et al*, 2011) would likely extend even further.

Mtr4 binds Rrp6 – Rrp47 via evolutionarily conserved interactions

The overall structure of Rrp6_N – Rrp47_N resembles a turn of a superhelix with a conserved concave surface that is formed by the $\alpha 1$ helix of Rrp6 and the $\alpha 2$ and $\alpha 3$ helices of Rrp47 and that provides the binding site for Mtr4_N (Fig 2B and 5A). Mtr4_N binds as a short α -helix (residues 6-11), with extended segments at both ends. Apolar residues of Mtr4 (Leu6, Phe7, Val9, Phe10, Val 15 and Leu17) contact hydrophobic residues of Rrp6 (Leu10, Ile14 and Val17) and Rrp47 (Tyr10, Tyr55, Phe62, Leu77,

Leu80 and Met87) (Fig 5B). In addition, Mtr4 Glu12 forms a salt bridge with Rrp6 Arg18, while Mtr4 Asp5 and Glu16 interact electrostatically with Lys84 and Lys6 of Rrp47 respectively. We tested the effect of mutating a set of the conserved interacting residues in *in vitro* binding assays. Isothermal titration calorimetry (ITC) experiments showed that Rrp6_N – Rrp47_{ΔC} bound to the Mtr4_N peptide with a K_d of 1.3 μM, but no binding to an Mtr4_N F7A, F10A mutant was detected (Fig 5C, left and central panel). Conversely, an Rrp6_N I14E, R18E – Rrp47_{ΔC} mutant showed no binding to wild-type Mtr4_N by ITC (Fig 5C, right panel). We note that there are also additional conserved residues, including Asp27 and Phe30 in the Rrp6 α_{short} helix and Rrp6 Glu90 and Asp97 on the convex surface of the superhelix (Fig. 5A). These residues do not contact Mtr4_N in the structure and consistently their mutation did not affect binding to Mtr4_N in ITC experiments (Fig E3A).

Impact of Rrp6_N-Rrp47_{ΔC} on RNA binding and degradation

The concave surface of Rrp6_N – Rrp47_N that binds Mtr4_N is highly positively charged (Fig 6A). Given these electrostatic properties and previous reports that Rrp47 binds RNA (Stead *et al*, 2007), we tested whether the interaction between Rrp6 and Rrp47 might also serve as an RNA-binding site (at least in the absence of Mtr4). Since from the structure of the N-terminal region of Rrp6 is expected to be unfolded in the absence of Rrp47, we compared Rrp6₁₋₅₁₈ – Rrp47_{ΔC} with Rrp6₁₂₂₋₅₁₈. We measured RNA-binding affinities by fluorescence anisotropy using fluorescein-labeled poly(A)₃₅ or poly(U)₃₀ RNAs and using a catalytic mutant of Rrp6 (Asp296 to Asn). In these experiments, we did not detect RNA binding to Rrp6_N – Rrp47_{ΔC} (Fig 6B), suggesting its positively charged concave surface is a protein-protein interaction site for Mtr4_N rather than an RNA-binding site. Rrp6_{122-518, D296A} and Rrp6_{1-518, D296A} –

Rrp47 Δ C bound RNA with a similar affinity in the low micromolar range (Fig 6B). In RNA degradation assays, the Rrp6₁₋₅₁₈ – Rrp47 Δ C complex showed somewhat lower activity as compared to that of Rrp6₁₂₂₋₅₁₈ (Fig 6C), indicating that the Rrp6_N-Rrp47 Δ C module subtly downregulates the enzymatic properties of the Rrp6 ribonuclease. Although the rationale for this effect is currently unclear, similar observations have been recently reported (Dedic *et al*, 2014; Barbosa *et al*, 2014).

We carried out a set of degradation assays of Rrp6 Δ NLS – Rrp47 Δ C in the presence of Mtr4, with and without the other subunits of the nuclear exosome complex (Fig E3B). We first tested a double-stranded substrate with a short 3' overhang (10 nucleotides) that from previous work is known to be inaccessible to the Rrp44 exoribonuclease when in the context of Exo-9 (Bonneau *et al*, 2009) (Fig E3B, upper panel). We also tested a double-stranded substrate with a long 3' overhang (35 nucleotides) that is accessible to the processive exoribonuclease activity of Rrp44 (Fig E3, lower panel). We found that the Rrp6-Rrp47 degradation properties on these substrates were not affected by the presence of Mtr4 (Fig E3B). Although we saw no significant effect of Mtr4 on the degradation of these substrates by either Rrp6 or Rrp44, we caution that it is possible that the helicase domain of Mtr4 might operate in the context of more complex RNA structures.

Structure-based mutations in the Rrp6 N-terminal domain result in 5.8S RNA processing defects *in vivo*

Loss of function *rrp6* and *rrp47* mutants shows strong defects in the 3' processing of 5.8S rRNA and box C/D snoRNAs (Briggs *et al*, 1998; Allmang *et al*, 1999a; Mitchell *et al*, 2003). These mutants accumulate the 5' external transcribed spacer (5' ETS) fragment that is released during early processing of the pre-rRNA transcript, as

well as truncated fragments of U3, 5S and snR13 as a result of impaired RNA surveillance processes (Briggs *et al*, 1998; Allmang *et al*, 1999a; Mitchell *et al*, 2003). To address the importance of the interaction between Mtr4 and the Rrp6 – Rrp47 heterodimer *in vivo*, we designed specific *rrp6* and *rrp47* mutants based on the structure of the Rrp6_N – Rrp47_N – Mtr4_N complex and analyzed the levels and integrity of the above RNAs in these mutants by Northern blot hybridization. Mutations were generated in the N-terminal region of Rrp6 and Rrp47 to either block the interaction with Mtr4 *in vitro* (*rrp6*_{I14E,R18E}, see Fig 5) or to alter other conserved surface residue pairs (*rrp6*_{D27R,F30R}, *rrp6*_{E90R,D97R}, *rrp47*_{Y55A,S59Y}, *rrp47*_{L77E,L80E} or *rrp47*_{A111Y,I115Y}).

The *rrp6*_{I14E,R18E}, *rrp6*_{D27R,F30R} and *rrp6*_{E90R,D97R} mutants showed an accumulation of the 3' extended “5.8S +30” species and a defect in the degradation of the 5' ETS fragment (see Fig 7A, lanes 4-6). The phenotype was stronger for the *rrp6*_{D27R,F30R} mutant and weaker with the *rrp6*_{I14E,R18E} mutant, but reproducible (see also Fig E4A). In contrast, no clear effect was seen on the 3' maturation of the snR38 snoRNA or the accumulation of degradation fragments from U3, snR13 or 5S rRNA in these mutants (denoted with asterisks in Fig 7A). These data are consistent with a partial loss of Rrp6 function in the *rrp6*_{I14E,R18E}, *rrp6*_{D27R,F30R} and *rrp6*_{E90R,D97R} mutants. All *rrp6* alleles complemented the temperature-sensitive growth phenotype of an *rrp6*Δ mutant (Fig 7B), were expressed comparably to the wild-type protein and had no effect on the expression level of Rrp47 (Fig 7C). Northern analyses of the *rrp47* mutants revealed no strong phenotypes, although a weak but reproducible accumulation of the 5.8S + 30 fragment was observed for the Y55A, S59Y and L77E, L80E mutants (Fig E4B). We concluded that mutation of conserved surface residues in the Rrp6 N-terminal domain, in particular D27 and F30, results in a clear defect in

5.8S rRNA maturation. It is currently unclear why conserved surface residues of Rrp6-Rrp47 that are not involved in Mtr4_N binding are important for function, but it is possible that they are involved in additional interactions within the nuclear exosome complex or with the substrate ribonucleoprotein particle.

Mtr4 and Rrp6 mutants show synergistic effects *in vivo*

C-terminally tagged Mtr4 fusion proteins can support cell growth (Huh *et al*, 2003; Ghaemmaghami *et al*, 2003). Indeed, we observed no clear growth defect for an *mtr4-gfp* strain when compared to an isogenic wild-type strain. Northern analyses of RNA isolated from the *mtr4-gfp* strain during growth in either minimal or rich medium did not show significant accumulation of the 5.8S + 30 fragment or the 3' extended forms of snoRNAs that are characteristic of *rrp6Δ* mutants (Briggs *et al*, 1998; Allmang *et al*, 1999a). However, the Northern analyses showed defects in the degradation of other structured RNAs, with a clear accumulation of the 5' ETS fragment that has been previously shown to accumulate upon Mtr4/Dob1 depletion (la Cruz *et al*, 1998) (see Fig 7A, lanes 7 and 8). These results indicated that the presence of the C-terminal GFP protein partially compromises the function of Mtr4, without causing a general affect on Rrp6-dependent processing or degradation pathways. We therefore generated an *rrp6Δ* allele in the haploid *mtr4-gfp* strain and tested for genetic interactions between the *mtr4-gfp* allele and the *rrp6* mutants.

Attempts to delete the *RRP6* gene in the *mtr4-gfp* strain directly were unsuccessful, but correct integrants were isolated when the *mtr4-gfp* strain had been transformed with a *URA3* plasmid encoding a functional Rrp6 fusion protein (Allmang *et al*, 1999b). Notably, deletion of the *RRP6* gene was also achieved in *mtr4-gfp* strains expressing *rrp6*_{D27R,F30R} and *rrp6*_{E90R,D97R} variants of the Rrp6 fusion

protein but not the *rrp6_{I14E,R18E}* mutant. To determine whether the *mtr4-gfp* *rrp6_{I14E,R18E}* double mutant is synthetic lethal, wild-type and *rrp6_{I14E,R18E}* mutant alleles were subcloned into the *LEU2* plasmid pRS415, transformed into the *mtr4-gfp* *rrp6* Δ plasmid shuffle strain and the resulting transformants were tested for growth on medium containing 5-fluoro-orotic acid (5 FOA). While transformation with the wild-type *RRP6* gene gave rise to viable colonies on 5 FOA medium, no growth was observed for the *mtr4-gfp* *rrp6* Δ strain after transformation with a plasmid encoding the *rrp6_{I14E,R18E}* mutant or the cloning vector (Fig 8A). We concluded that the *mtr4-gfp* strain is dependent upon Rrp6 for cell growth.

To determine whether the Rrp6/Mtr4 interaction in yeast is blocked by the *rrp6_{I14E, R18E}* mutation, pull-downs were performed on lysates from *mtr4-gfp* strains expressing plasmid-encoded, zz epitope-tagged wild-type or mutant Rrp6 fusion proteins (in addition to the endogenously encoded Rrp6). Mtr4-gfp was bound to the wild-type zz-Rrp6 protein, but not the I14E, R18E mutant (Fig 8B, left panel). We then addressed whether mutation of the N-terminal region of Mtr4 also causes a block in the Rrp6/Mtr4 interaction *in vivo*. Immobilized zz-Rrp6 protein retained the wild-type Mtr4-gfp protein, whereas binding of the *mtr4-gfp_{F7A,F10A}* mutant was only slightly above background levels (Fig 8B, right panel). These data support the conclusion that the structurally defined Rrp6_N - Rrp47_N - Mtr4_N complex forms the principal interaction between Rrp6 and Mtr4 in yeast.

If the synthetic lethal phenotype observed for the *mtr4-gfp* *rrp6_{I14E, R18E}* mutant (Fig 8A) is due to loss of interaction between Mtr4 and Rrp6, a strong synergistic effect would be predicted upon introduction of the F7A, F10A mutation in the *mtr4-gfp* mutant. Indeed, both the *mtr4-gfp* and the *mtr4_{F7A, F10A}* mutants grew comparably to the wild-type strain, whereas the strain expressing an Mtr4-gfp fusion protein

bearing the F7A, F10A mutation was nonviable (Fig 8C). We concluded that the strong synergistic effects observed in strains expressing a C-terminal Mtr4-gfp fusion protein in combination with either the Rrp6 I14E, R18E mutation (that impairs the interaction with the N-terminus of Mtr4) or the Mtr4 F7A,F10A mutation (that impairs the interaction with the N-terminal domains of Rrp6-Rrp47) is due to loss of binding. The very C-terminus of Mtr4 is embedded within the base of the DExH core of the helicase, where the 3' end of an RNA substrate is expected to emerge after unwinding (Jackson *et al*, 2010; Weir *et al*, 2010). Collectively, these data suggest that the base of Mtr4 is also engaged in interactions within the nuclear exosome complex and that linking the C-terminus of Mtr4 to a GFP protein weakens this interaction.

Northern analyses of the viable *mtr4-gfp rrp6_{D27R,F30R}* and *mtr4-gfp rrp6_{E90R,D97R}* double mutants revealed a strong synergistic block in the degradation of some RNAs, including the 5' ETS fragment and truncated fragments of U3, snR13 and 5S rRNA (Fig 7A, lanes 9 and 10). In contrast, the defect in 5.8S rRNA maturation seen in the *rrp6_{D27R,F30R}* or *rrp6_{E90R,E97R}* mutants was not exacerbated in the *mtr4-gfp rrp6* double mutants. This suggests that *mtr4-gfp rrp6* mutants may be defective in RNA surveillance mechanisms, rather than 5.8S rRNA or snoRNA processing.

Discussion

The interaction of Rrp6 and Rrp47 is known to stabilize the individual proteins *in vivo* and to influence their function in exosome-mediated RNA processing and turnover pathways. The molecular basis for these effects, however, has remained unclear. Here, we show that the N-terminal domains of Rrp6 and Rrp47 assemble into a globular

heterodimer with an elaborate architecture formed by intertwined pairs of α -helices. The interlocked Rrp6_N – Rrp47_N structure explains why heterodimer formation leads to stabilization and to functional interdependence. In isolation, the individual proteins are expected to be partially unfolded and aggregated. As a 1:1 complex, they form a composite molecular surface for the direct recruitment of the N-terminal region of Mtr4, which binds via a set of evolutionarily conserved interactions. Together with the observation that Rrp6 and Rrp47 assemble only after they are independently imported into the nucleus (Feigenbutz *et al*, 2013b), these results rationalize how the cell might avoid the untimely recruitment of Mtr4 to the exosome in the cytoplasm.

The Rrp6_N – Rrp47_N heterodimer does not undergo significant conformational changes upon Mtr4_N binding and thus appears to function as a rather rigid platform. The structural analysis and *in vivo* data suggest that this platform also contains docking sites for other interaction partners whose identities remain to be explored. It is also likely that Rrp6, Rrp47 and Mtr4 are engaged in additional, albeit weaker, contacts in the context of the nuclear exosome complex. Although we did not observe direct interactions between Rrp6 – Rrp47 and Mpp6 and between Mtr4 and Mpp6, as has been reported for the human orthologues (Schilders *et al*, 2007), it is possible that the yeast proteins might engage in analogous contacts but without the high affinity required for detection in the *in vitro* reconstitution assays we used. Indeed, synthetic lethal mutations in *S. cerevisiae* support the presence of redundant interactions among the yeast cofactors of the nuclear exosome (Milligan *et al*, 2008; Garland *et al*, 2013 and Fig 8A). The presence of additional weak interactions would also rationalize why Mtr4 would be able to carry out at least part of its functions *in vivo* in the absence of Rrp6 and Rrp47, as can be inferred from the severity of the corresponding knock-out

studies (la Cruz *et al*, 1998; Briggs *et al*, 1998; Mitchell *et al*, 2003). The emerging picture is that Rrp6, Rrp47, Mpp6 and Mtr4 assemble together with Exo-10 with a combination of high-affinity interactions and additional intermolecular contacts to form a functional nuclear complex (Fig 9). Understanding how the nuclear exosome complex is structured and how it coordinates the multiple catalytic activities of core components and cofactors awaits future studies.

Materials and methods

Protein purification

S. cerevisiae Mtr4 full-length, Mtr4_{Δ80} and the *Neurospora crassa* Mtr4 orthologue FRH were expressed and purified according to the protocol in Weir *et al* 2010. Exo-9 and Rrp44 were expressed and purified as in Makino *et al* 2013a. All other *S. cerevisiae* proteins purified in this study were expressed recombinantly using *E. coli* BL21-Gold (DE3) pLysS cells (Stratagene) grown in TB medium and induced overnight at 18° C. Rrp6_N, Rrp6_{ΔN} and Mtr4₈₀ were expressed as His-tagged proteins. Rrp6_N – Rrp47_N, Rrp6_N – Rrp47_{ΔC} and Rrp6_{ΔNLS} – Rrp47 complexes were co-expressed such that the Rrp6 constructs bear an N-terminal His tag while the Rrp47 constructs are untagged. The proteins were purified using Cobalt-based (or Nickel for Mtr4₈₀) affinity chromatography, followed by cleavage of the His-tag with the appropriate protease (Human Rhinovirus 3C protease for Rrp6_N, Rrp6_N – Rrp47_N, Rrp6_N – Rrp47_{ΔC}, tobacco etch virus (TEV) protease for Mtr4₈₀, Rrp6_{ΔNLS} – Rrp47 and small ubiquitin-like modifier (SUMO) protease for Rrp6_{ΔN}). Protease treated-Rrp6_{ΔN} was loaded on the affinity column a second time to remove uncleaved species.

After affinity purification, all samples (with the exception of Mtr4₈₀) were subjected to anion exchange chromatography (HiTrap Q HP, GE Healthcare). Rrp6_{ΔN} and Rrp6_{ΔNLS} – Rrp47 were further purified over a HiTrap Heparin Sepharose HP column (GE Healthcare).

Size-exclusion chromatography (SEC) on a Superdex 200 or Superdex 75 column (GE Healthcare) was performed as a final step of purification for all proteins. Rrp6_N and complexes of this construct were finally purified in buffer A (20 mM Tris pH 7.5, 100 mM NaCl) supplemented with reducing agents. An additional 10% glycerol was added to the size-exclusion buffer when purifying Rrp6_N and Rrp6_{ΔNLS} – Rrp47. Mtr4₈₀ was purified in buffer A supplemented with an additional 50 mM NaCl and 2 mM DTT. Size exclusion for Rrp6_{ΔN} was performed in buffer B (20 mM MES pH 6.0, 250 mM NaCl, 10% glycerol, 2 mM DTT). Rrp6 mutants were verified by DNA sequencing, and purified using the protocol for the wild-type protein. Yeast Rrp47_{ΔC} and Mpp6 were expressed as recombinant GST-tagged (3C- or TEV protease-cleavable, respectively) proteins in conditions similar to those described above. The proteins were purified by affinity chromatography on Glutathione Sepharose resin (Clontech). Tag cleavage was followed by ion-exchange chromatography (HiTrap SP Sepharose HP column, GE Healthcare) and SEC (in buffer A supplemented with 1 mM DTT and 10% glycerol) for Rrp47_{ΔC}. Tag-cleaved Mpp6 was purified over a HiTrap Heparin Sepharose HP column (GE Healthcare) as the final step.

Crystallization and structure determination

Crystals of yeast Rrp6_N – Rrp47_{ΔC} were grown at 20° C by sitting-drop vapor diffusion from drops formed by equal volumes of protein (at 18 mg/ml in size

exclusion buffer comprising 20 mM Tris, 100 mM NaCl and 1 mM DTT) and of crystallization solution (1.8 M $(\text{NH}_4)_2\text{SO}_4$, 125 mM NaCl and 100 mM Na-cacodylate pH 5.8). For heavy-atom derivatization, native Rrp6_N – Rrp47_{ΔC} crystals (grown in 2.05 M $(\text{NH}_4)_2\text{SO}_4$, 125 mM NaCl and 100 mM Na-cacodylate pH 6.4) were soaked for 15 minutes in crystallization solution supplemented with 1 mM Ta₆Br₁₄ prior to cryoprotection. Optimized Se-Met derivatized crystals were obtained in 2.0 M $(\text{NH}_4)_2\text{SO}_4$, 200 mM NaCl and 100 mM Na-cacodylate pH 6.2. Crystals were cryoprotected with crystallization solution supplemented with 24% glycerol for the native crystals and 17.5% glycerol for the Ta soaked and Se-Met derivatized crystals prior to cryo-cooling and data collection.

Yeast Rrp6_N – Rrp47_N complex was mixed with a 1.5-fold molar excess of Mtr4_N (synthesized peptide (H)-MDSTDLFDVFEETPVELPTK-(NH₂); D20K substitution for synthesis strategy and solubility reasons) and 5 mM YCl₃ and incubated at room temperature for 10 minutes. Crystals of the Rrp6_N – Rrp47_N – Mtr4_N complex were grown at 20° C by sitting-drop vapor diffusion from drops formed by equal volumes of complex (at 27 mg/ml in size-exclusion buffer comprising 20 mM Tris, 100 mM NaCl and 0.5 mM TCEP) and crystallization solution (12% PEG 1000, 0.1M imidazole pH 7.5 and 0.125 M calcium acetate). Crystals were cryoprotected in 19% PEG 1000, 0.1M imidazole pH 7.5, 0.125 M calcium acetate, 5 mM YCl₃, 12% glycerol and supplemented with 0.5 mM Mtr4_N peptide. Data were collected at the ID23-2 beamline of the European Synchrotron Radiation Facility (ESRF, Grenoble, France) and at the PXII and PXIII beamlines of the Swiss Light Source (SLS) (Villigen, Switzerland) and processed using XDS (Kabsch, 2010).

The Rrp6_N – Rrp47_{ΔC} structure was solved at low resolution (5.2Å) by SAD with SHELX (Sheldrick, 2008) and HKL2MAP (Pape & Schneider, 2004) using the anomalous Ta signal. Identifiable α -helices were manually placed with Coot (Emsley *et al*, 2010) and used as a starting model for SAD-MR by exploiting the anomalous Se signal using the program Phenix AutoSol (Terwilliger *et al*, 2009). After manual chain tracing, the model was completed with Coot and refined against the native data using phenix.refine (Afonine *et al*, 2012). The Rrp6_N – Rrp47_N – Mtr4_N structure was solved by SAD-MR using Phaser (McCoy *et al*, 2007) with parts of the Rrp6_N – Rrp47_{ΔC} model as a search model and AutoSol using the anomalous signal from yttrium. Merohedral twinning generated by a two-fold axis perpendicular to a crystallographic 3-fold axis of the trigonal space group became apparent by the poor quality of the electron density for one of the three copies of the complex in the asymmetric unit. The twin law (-h,-k,l) and twinning fraction (0.5, perfect twin) was determined using phenix.xtriage (Adams *et al*, 2010). After manual tracing of the Mtr4_N sequence, the model was completed using Coot and refined against twinned data using phenix.refine. Several Yttrium ions form clusters surrounded by electron density that likely corresponds to a negatively charged loop of Rrp6 (residues 63-73).

Size exclusions chromatography assay

Equimolar amounts of purified proteins as indicated (500 pmol for Fig 1C and D, 700 pmol otherwise) were diluted in a total injection volume of 25 μ l in SEC buffer A supplemented with 2 mM DTT. Samples were incubated for 1 hour on ice to allow complex formation. Increase in particle size upon complex formation was assayed by comparing the retention volumes in SEC on a Superdex 200 Increase 3.2/300 (GE

Healthcare). Composition of the SEC peak fractions were analyzed by SDS-PAGE and visualized by Coomassie-staining (percentage of the SDS-PAGE depended on protein sample size).

Fluorescence anisotropy

Fluorescence anisotropy measurements were performed with a 5'-6-carboxy-fluorescein (6-FAM)-labeled poly(A)₃₅ or poly(U)₃₀ RNA at 20° C in 50 µl reactions on a Genios Pro (Tecan). The RNA was dissolved to a concentration of 10 nM (1 nM for Rrp6_N, D296N – Rrp47) and incubated with Rrp6 or the Rrp6 – Rrp47 complexes at different concentrations in a buffer containing 20 mM Tris pH 7.5, 100 mM NaCl, and 1 mM DTT. The excitation and emission wavelengths were 485 nm and 535 nm, respectively. Each titration point was measured three times using ten reads with an integration time of 40 µ s. The data were analyzed by nonlinear regression fitting using the BIOEQS software (Royer, 1993).

Isothermal titration calorimetry (ITC)

Rrp6_N – Rrp47_{ΔC} wild-type and mutant proteins were dialyzed overnight in the same buffer that was used to dissolve the lyophilized Mtr4_N peptide (20 mM Hepes, pH 7.5, 100 mM NaCl, 0.5 mM TCEP). ITC experiments were carried out at 20°C with a iTC-200 MicroCal calorimeter (GE healthcare). The MicroCal cell was filled with Rrp6_N – Rrp47_{ΔC} at 50 µM concentration and stirred at 800 rpm. For each titration, Mtr4_N was injected into the cell 20 times in 2 µl volumes per injection at the same intervals of time (4 min). The concentration of Mtr4_N in the syringe (500 µM) was 10 times the concentration of the protein sample in the cell. The released heat was obtained by integrating the calorimetric output curves and was corrected for the effect

of dilution by subtraction of the value of the last injection as background. As control for all ITC measurements, the injectant was titrated into buffer. The K_d values and binding ratios were calculated with the Origin (V7) software supplied with the calorimeter. We used the same protocol to measure the K_d of the Rrp6 and the Mtr4 mutants.

Nuclease Assay

The exonuclease activity assay in figure 6C was carried out at 30° C in a buffer containing 50 mM HEPES pH 7.5, 50 mM NaCl, 5 mM magnesium diacetate, 10% (v/v) glycerol, 0.1% (v/v) NP40 and 1 mM DTT. The reactions contained protein at a final concentration of 2 nM while the concentration of RNA substrates was 200 nM. Substrates were verified by native gel electrophoresis. Two microliter aliquots from a 10 μ l total reaction volume were taken at indicated time points and quenched by addition of 14 μ l loading dye consisting of 10 mM EDTA, 0.1% (w/v) bromophenol blue, and 0.1% (w/v) xylene cyanole FF in formamide. The 0 - time point was taken before adding the protein. Reaction products were boiled for 5 minutes immediately before being resolved on a 20% acrylamide gel containing 8 M urea and visualized by phosphorimaging.

Plasmids and Yeast Strains

Yeast expression plasmids encoding either an N-terminal zz fusion of Rrp6 under the control of the *RRP4* promoter (Allmang *et al*, 1999b), or containing a genomic clone of the *RRP6* gene and lacking the *CEN6* element from the vector backbone (Feigenbutz *et al*, 2013a), have been reported previously. Expression of the N-terminal zz-Rrp6 fusion protein from the *RRP4* promoter is comparable to the

endogenous expression level of the C-terminal TAP-tagged protein (Stead *et al*, 2007). The *RRP47* genomic clone used in this study is described in Costello *et al*. (Costello *et al*, 2011). The *MTR4* construct pAv675 (Jackson *et al*, 2010) was kindly provided by Ambro van Hoof (University of Texas Health Science Center, Houston). The construct encoding *mtr4-gfp* was cloned in yeast by homologous recombination, using *Hind* III linearized pAv675 (after deletion of the *Hind* III polylinker site) and a PCR amplicon encompassing the *mtr4-gfp::HIS3* allele. The isolated plasmid was confirmed by sequencing the *mtr4/GFP* junction along the complete length of the PCR product. Point mutations were introduced into the *RRP6*, *RRP47* and *MTR4* ORFs in these constructs by site-directed mutagenesis using the Quikchange kit (Agilent Technologies) and validated by sequence analysis. Plasmid inserts encoding the N-terminal epitope-tagged wild-type *RRP6* and *rrp6^{114E,18E}* mutants were subcloned into pRS415 (Stratagene) for the plasmid shuffle assay. The *rrp6Δ::KANMX4* allele was amplified by PCR and integrated into the *mtr4-gfp* strain by homologous recombination after initial transformation with plasmids encoding zz-Rrp6 fusion proteins. Correct integrants were identified by PCR amplification of genomic DNA.

The *mtr4-gfp* strain (Huh *et al*, 2003) was obtained from Invitrogen. The *mtr4* plasmid shuffle strain yAv1151 (Jackson *et al*, 2010) was kindly provided by Ambro van Hoof. Isogenic wild-type and *rrp6Δ* strains were obtained from Euroscarf (University of Frankfurt, Germany). The *rrp47-zz* and *rrp47-zz rrp6Δ* strains have been previously reported (Mitchell *et al*, 2003). Yeast strains were routinely cultured at 30 °C in SD selective minimal medium (2% glucose, 0.5% ammonium sulphate, 0.17% yeast nitrogen base) supplemented with appropriate amino acids and bases, or in YPD medium (2% glucose, 2% peptone, 1% yeast extract). Spot growth assays

were performed on selective solid minimal medium or medium containing 5-fluoroorotic acid (5 FOA) using 10-fold serial dilutions of freshly saturated pre-cultures. Plates were photographed after incubation for 3 days.

RNA Analyses

Total cellular RNA was isolated from strains harvested during early log growth and resolved by electrophoresis through 8% polyacrylamide gels containing 50% urea. After transfer to Hybond N⁺ membranes (GE Healthcare), the RNA was hybridized with 5'-[³²P] labeled oligonucleotide probes complementary to the ITS2 region of the pre-rRNA transcript (tgagaaggaaatgacgct), 5.8S rRNA (gcgttggtcatcgatgc), the 5' ETS region of the pre-rRNA (cgctgctcaccaatgg), snR38 (gagaggttacctattattaccattcagacaggataactg), U3 (ttcggtttctcactctgggggtac), snR13 (caccgttactgatttggc), 5S (ctactcggtcaggctc), *SCR1* (aaggaccagaactaccttg) and U6 (atctctgtattgtttcaaattgaccaa). Hybridized blots were placed under phosphor storage screens and the data was captured using a Personal Molecular Imager (BioRad). Nonsaturated images were adjusted for signal level and window using ImageJ (NIH, USA). RNA hybridization signals were quantified using ImageJ and normalized to the expression level of 5S rRNA.

Protein Analyses

For protein expression analyses, total cellular protein was prepared by alkaline/SDS lysis followed by TCA precipitation. Extracts were resolved by SDS/PAGE, transferred to Hybond C extra membranes (GE Healthcare) and incubated with a rabbit anti-Rrp6 antiserum (Mitchell *et al*, 2003) or mouse anti-Pgk1 (clone 22C5D8, Life Technologies) primary antibody, followed by either goat anti-rabbit (A4914,

Sigma) or goat anti-mouse (1706516, BioRad) HRP-conjugated secondary antibodies. The Mtr4-gfp fusion protein was detected using the anti-GFP antibody. The Rrp47-zz fusion protein was detected directly using the PAP antibody conjugate (P1291, Sigma). ECL images were captured using a G:Box iChemi XL system (Syngene) and adjusted for the signal level and window using ImageJ.

For the pull-down experiments, yeast were lysed in 50 mM HEPES pH 7.4, 50 mM KCl, 5 mM MgCl₂, 10 % glycerol, 1 mM PMSF. Lysates were clarified by centrifugation at 13,000 g for 30 minutes, normalized for A₂₈₀ units, and passed through ~ 200 µl IgG sepharose fast flow beads (GE Healthcare). The beads were washed 5 times with 1 ml wash buffer (50 mM HEPES pH 7.4, 100 mM KCl, 5 mM MgCl₂, 0.1% NP-40, 1 mM DTT) and the retained material was eluted with 0.5 M acetic acid. Eluates were resolved through 10 % SDS-PAGE gels and analyzed by western blotting, as described above.

Data deposition

The coordinates and structure factors have been deposited in the Protein Data Bank with accession codes xxx for the Rrp6_N – Rrp47_{ΔC} structure and yyy for the Rrp6_N – Rrp47_N – Mtr4_N structure.

Acknowledgements

We would like to thank the Max Planck Institute of Biochemistry (MPIB) Core Facility for synthesizing the peptides used in the study and for mass spectrometry analysis; the MPIB Crystallization Facility for crystallization screenings; the beamline scientists at the SLS and the ESRF for assistance with data collection. We also thank Marc Baumgärtner, Tatjana Krywcun and Petra Birle for technical assistance, and

members of our labs for useful discussions and critical reading of the manuscript. This study was supported by the Max Planck Gesellschaft, the European Commission (ERC Advanced Investigator Grant 294371 and Marie Curie ITN RNPnet) and the Deutsche Forschungsgemeinschaft (DFG SFB646, SFB1035, GRK1721, FOR1680 and CIPSM) to EC and by a research grant from the Wellcome Trust (08836/Z/09/Z) to P.M. We thank David Tollervey (University of Edinburgh) for the yeast Rrp6 antiserum and Ambro van Hoof (University of Texas Health Science Center, Houston) for mtr4 strains and plasmids.

Author contributions

B.S. carried out the structural analyses, B.S., D.M. and S.F. the *in vitro* biochemical analyses, C.B the biophysical analyses, M.F. and P.M. the *in vivo* experiments. B.S., E.C. and P.M. wrote the manuscript

Conflict of interest

The authors declare that they have no conflict of interest.

References

- Adams PD, Afonine PV, Bunkóczi G, Chen VB, Davis IW, Echols N, Headd JJ, Hung LW, Kapral GJ, Grosse-Kunstleve RW, McCoy AJ, Moriarty NW, Oeffner R, Read RJ, Richardson DC, Richardson JS, Terwilliger TC & Zwart PH (2010) PHENIX: a comprehensive Python-based system for macromolecular structure solution. *Acta Crystallogr D Biol Crystallogr* **66**: 213–221
- Afonine PV, Grosse-Kunstleve RW, Echols N, Headd JJ, Moriarty NW, Mustyakimov M, Terwilliger TC, Urzhumtsev A, Zwart PH & Adams PD (2012) Towards automated crystallographic structure refinement with phenix.refine. *Acta Crystallogr D Biol Crystallogr* **68**: 352–367
- Allmang C, Kufel J, Chanfreau G, Mitchell P, Petfalski E & Tollervey D (1999a) Functions of the exosome in rRNA, snoRNA and snRNA synthesis. *EMBO J* **18**: 5399–5410

- Allmang C, Petfalski E, Podtelejnikov A, Mann M, Tollervey D & Mitchell P (1999b) The yeast exosome and human PM-Scl are related complexes of 3' → 5' exonucleases. *Genes Dev* **13**: 2148–2158
- Anderson JS & Parker RP (1998) The 3' to 5' degradation of yeast mRNAs is a general mechanism for mRNA turnover that requires the SKI2 DEVH box protein and 3' to 5' exonucleases of the exosome complex. *EMBO J* **17**: 1497–1506
- Araki Y, Takahashi S, Kobayashi T, Kajiho H, Hoshino S & Katada T (2001) Ski7p G protein interacts with the exosome and the Ski complex for 3'-to-5' mRNA decay in yeast. *EMBO J* **20**: 4684–4693
- Barbosa RL, Legrand P, Wien F, Pineau B, Thompson A & Guimarães BG (2014) RRP6 from *Trypanosoma brucei*: crystal structure of the catalytic domain, association with EAP3 and activity towards structured and non-structured RNA substrates. *PLoS ONE* **9**: e89138
- Bernstein J & Toth EA (2012) Yeast nuclear RNA processing. *World J Biol Chem* **3**: 7–26
- Bonneau F, Basquin J, Ebert J, Lorentzen E & Conti E (2009) The yeast exosome functions as a macromolecular cage to channel RNA substrates for degradation. *Cell* **139**: 547–559
- Bousquet-Antonelli C, Presutti C & Tollervey D (2000) Identification of a regulated pathway for nuclear pre-mRNA turnover. *Cell* **102**: 765–775
- Briggs MW, Burkard KT & Butler JS (1998) Rrp6p, the yeast homologue of the human PM-Scl 100-kDa autoantigen, is essential for efficient 5.8 S rRNA 3' end formation. *J Biol Chem* **273**: 13255–13263
- Burkard KT & Butler JS (2000) A nuclear 3'-5' exonuclease involved in mRNA degradation interacts with Poly(A) polymerase and the hnRNA protein Npl3p. *Mol Cell Biol* **20**: 604–616
- Butler JS & Mitchell P (2011) Rrp6, rrp47 and cofactors of the nuclear exosome. *Adv Exp Med Biol* **702**: 91–104
- Callahan KP & Butler JS (2008) Evidence for core exosome independent function of the nuclear exoribonuclease Rrp6p. *Nucleic Acids Res* **36**: 6645–6655
- Chlebowski A, Lubas M, Jensen TH & Dziembowski A (2013) RNA decay machines: the exosome. *Biochim Biophys Acta* **1829**: 552–560
- Costello JL, Stead JA, Feigenbutz M, Jones RM & Mitchell P (2011) The C-terminal Region of the Exosome-associated Protein Rrp47 Is Specifically Required for Box C/D Small Nucleolar RNA 3'-Maturation. *Journal of Biological Chemistry* **286**: 4535–4543
- Cristodero M, Böttcher B, Diepholz M, Scheffzek K & Clayton C (2008) The *Leishmania tarentolae* exosome: purification and structural analysis by electron microscopy. *Mol Biochem Parasitol* **159**: 24–29

- Davis CA & Ares M (2006) Accumulation of unstable promoter-associated transcripts upon loss of the nuclear exosome subunit Rrp6p in *Saccharomyces cerevisiae*. *Proc Natl Acad Sci USA* **103**: 3262–3267
- Dedic E, Seweryn P, Jonstrup AT, Flygaard RK, Fedosova NU, Hoffmann SV, Boesen T & Brodersen DE (2014) Structural analysis of the yeast exosome Rrp6p-Rrp47p complex by small-angle X-ray scattering. *Biochem. Biophys. Res. Commun.* **450**: 634–640
- Dziembowski A, Lorentzen E, Conti E & Séraphin B (2007) A single subunit, Dis3, is essentially responsible for yeast exosome core activity. *Nat Struct Mol Biol* **14**: 15–22
- Emsley P, Lohkamp B, Scott WG & Cowtan K (2010) Features and development of Coot. *Acta Crystallogr D Biol Crystallogr* **66**: 486–501
- Feigenbutz M, Garland W, Turner M & Mitchell P (2013a) The exosome cofactor Rrp47 is critical for the stability and normal expression of its associated exoribonuclease Rrp6 in *Saccharomyces cerevisiae*. *PLoS ONE* **8**: e80752
- Feigenbutz M, Jones R, Besong TMD, Harding SE & Mitchell P (2013b) Assembly of the yeast exoribonuclease Rrp6 with its associated cofactor Rrp47 occurs in the nucleus and is critical for the controlled expression of Rrp47. *Journal of Biological Chemistry* **288**: 15959–15970
- Garland W, Feigenbutz M, Turner M & Mitchell P (2013) Rrp47 functions in RNA surveillance and stable RNA processing when divorced from the exoribonuclease and exosome-binding domains of Rrp6. *RNA* **19**: 1659–1668
- Ghaemmaghami S, Huh W-K, Bower K, Howson RW, Belle A, Dephoure N, O'Shea EK & Weissman JS (2003) Global analysis of protein expression in yeast. *Nature* **425**: 737–741
- Gudipati RK, Xu Z, Lebreton A, Seraphin B, Steinmetz LM, Jacquier A & Libri D (2012) Extensive degradation of RNA precursors by the exosome in wild-type cells. *Mol Cell* **48**: 409–421
- Halbach F, Reichelt P, Rode M & Conti E (2013) The yeast ski complex: crystal structure and RNA channeling to the exosome complex. *Cell* **154**: 814–826
- Halbach F, Rode M & Conti E (2012) The crystal structure of *S. cerevisiae* Ski2, a DExH helicase associated with the cytoplasmic functions of the exosome. *RNA* **18**: 124–134
- Hilleren P, McCarthy T, Rosbash M, Parker R & Jensen TH (2001) Quality control of mRNA 3'-end processing is linked to the nuclear exosome. *Nature* **413**: 538–542
- Huh W-K, Falvo JV, Gerke LC, Carroll AS, Howson RW, Weissman JS & O'Shea EK (2003) Global analysis of protein localization in budding yeast. *Nature* **425**: 686–691
- Jackson RN, Klauer AA, Hintze BJ, Robinson H, van Hoof A & Johnson SJ (2010)

- The crystal structure of Mtr4 reveals a novel arch domain required for rRNA processing. *EMBO J* **29**: 2205–2216
- Januszyk K, Liu Q & Lima CD (2011) Activities of human RRP6 and structure of the human RRP6 catalytic domain. *RNA* **17**: 1566–1577
- Kabsch W (2010) Integration, scaling, space-group assignment and post-refinement. *Acta Crystallogr D Biol Crystallogr* **66**: 133–144
- Kadaba S, Krueger A, Trice T, Krecic AM, Hinnebusch AG & Anderson J (2004) Nuclear surveillance and degradation of hypomodified initiator tRNA^{Met} in *S. cerevisiae*. *Genes Dev* **18**: 1227–1240
- Klauer AA & van Hoof A (2013) Genetic interactions suggest multiple distinct roles of the arch and core helicase domains of Mtr4 in Rrp6 and exosome function. *Nucleic Acids Res* **41**: 533–541
- la Cruz de J, Kressler D, Tollervey D & Linder P (1998) Dob1p (Mtr4p) is a putative ATP-dependent RNA helicase required for the 3' end formation of 5.8S rRNA in *Saccharomyces cerevisiae*. *EMBO J* **17**: 1128–1140
- LaCava J, Houseley J, Saveanu C, Petfalski E, Thompson E, Jacquier A & Tollervey D (2005) RNA degradation by the exosome is promoted by a nuclear polyadenylation complex. *Cell* **121**: 713–724
- Liu J-J, Bratkowski MA, Liu X, Niu C-Y, Ke A & Wang H-W (2014) Visualization of distinct substrate-recruitment pathways in the yeast exosome by EM. *Nat Struct Mol Biol* **21**: 95–102
- Liu Q, Greimann JC & Lima CD (2006) Reconstitution, activities, and structure of the eukaryotic RNA exosome. *Cell* **127**: 1223–1237
- Lorentzen E, Basquin J, Tomecki R, Dziembowski A & Conti E (2008) Structure of the active subunit of the yeast exosome core, Rrp44: diverse modes of substrate recruitment in the RNase II nuclease family. *Mol Cell* **29**: 717–728
- Lubas M, Christensen MS, Kristiansen MS, Domanski M, Falkenby LG, Lykke-Andersen S, Andersen JS, Dziembowski A & Jensen TH (2011) Interaction profiling identifies the human nuclear exosome targeting complex. *Mol Cell* **43**: 624–637
- Makino DL, Baumgärtner M & Conti E (2013a) Crystal structure of an RNA-bound 11-subunit eukaryotic exosome complex. *Nature* **495**: 70–75
- Makino DL, Halbach F & Conti E (2013b) The RNA exosome and proteasome: common principles of degradation control. *Nat Rev Mol Cell Biol* **14**: 654–660
- Malet H, Topf M, Clare DK, Ebert J, Bonneau F, Basquin J, Drazkowska K, Tomecki R, Dziembowski A, Conti E, Saibil HR & Lorentzen E (2010) RNA channelling by the eukaryotic exosome. *EMBO Rep* **11**: 936–942
- McCoy AJ, Grosse-Kunstleve RW, Adams PD, Winn MD, Storoni LC & Read RJ

- (2007) Phaser crystallographic software. *J Appl Crystallogr* **40**: 658–674
- Midtgaard SF, Assenholt J, Jonstrup AT, Van LB, Jensen TH & Brodersen DE (2006) Structure of the nuclear exosome component Rrp6p reveals an interplay between the active site and the HRDC domain. *Proc Natl Acad Sci USA* **103**: 11898–11903
- Milligan L, Decourty L, Saveanu C, Rappsilber J, Ceulemans H, Jacquier A & Tollervey D (2008) A yeast exosome cofactor, Mpp6, functions in RNA surveillance and in the degradation of noncoding RNA transcripts. *Mol Cell Biol* **28**: 5446–5457
- Mitchell P & Tollervey D (2003) An NMD pathway in yeast involving accelerated deadenylation and exosome-mediated 3'→5' degradation. *Mol Cell* **11**: 1405–1413
- Mitchell P, Petfalski E, Houalla R, Podtelejnikov A, Mann M & Tollervey D (2003) Rrp47p is an exosome-associated protein required for the 3' processing of stable RNAs. *Mol Cell Biol* **23**: 6982–6992
- Neil H, Malabat C, d'Aubenton-Carafa Y, Xu Z, Steinmetz LM & Jacquier A (2009) Widespread bidirectional promoters are the major source of cryptic transcripts in yeast. *Nature* **457**: 1038–1042
- Pape T & Schneider TR (2004) HKL2MAP: a graphical user interface for macromolecular phasing with SHELXprograms. *J Appl Crystallogr* **37**: 843–844
- Peng WT, Robinson MD, Mnaimneh S, Krogan NJ, Cagney G, Morris Q, Davierwala AP, Grigull J, Yang X, Zhang W, Mitsakakis N, Ryan OW, Datta N, Jovic V, Pal C, Canadien V, Richards D, Beattie B, Wu LF, Altschuler SJ, et al (2003) A panoramic view of yeast noncoding RNA processing. *Cell* **113**: 919–933
- Royer CA (1993) Improvements in the numerical analysis of thermodynamic data from biomolecular complexes. *Anal. Biochem.* **210**: 91–97
- Schaeffer D, Clark A, Klauer AA, Tsanova B & van Hoof A (2011) Functions of the cytoplasmic exosome. *Adv Exp Med Biol* **702**: 79–90
- Schilders G, van Dijk E & Pruijn GJM (2007) C1D and hMtr4p associate with the human exosome subunit PM/Scf-100 and are involved in pre-rRNA processing. *Nucleic Acids Res* **35**: 2564–2572
- Schmid M & Jensen TH (2008) The exosome: a multipurpose RNA-decay machine. *Trends Biochem Sci* **33**: 501–510
- Schneider C & Tollervey D (2013) Threading the barrel of the RNA exosome. *Trends Biochem Sci* **38**: 485–493
- Sheldrick GM (2008) A short history of SHELX. *Acta Crystallogr., A, Found. Crystallogr.* **64**: 112–122
- Stead JA, Costello JL, Livingstone MJ & Mitchell P (2007) The PMC2NT domain of

the catalytic exosome subunit Rrp6p provides the interface for binding with its cofactor Rrp47p, a nucleic acid-binding protein. *Nucleic Acids Res* **35**: 5556–5567

- Stuparevic I, Mosrin-Huaman C, Hervouet-Coste N, Remenaric M & Rahmouni AR (2013) Cotranscriptional recruitment of RNA exosome cofactors Rrp47p and Mpp6p and two distinct Trf-Air-Mtr4 polyadenylation (TRAMP) complexes assists the exonuclease Rrp6p in the targeting and degradation of an aberrant messenger ribonucleoprotein particle (mRNP) in yeast. *Journal of Biological Chemistry* **288**: 31816–31829
- Synowsky SA, van Wijk M, Raijmakers R & Heck AJR (2009) Comparative multiplexed mass spectrometric analyses of endogenously expressed yeast nuclear and cytoplasmic exosomes. *J Mol Biol* **385**: 1300–1313
- Terwilliger TC, Adams PD, Read RJ, McCoy AJ, Moriarty NW, Grosse-Kunstleve RW, Afonine PV, Zwart PH & Hung LW (2009) Decision-making in structure solution using Bayesian estimates of map quality: the PHENIX AutoSol wizard. *Acta Crystallogr D Biol Crystallogr* **65**: 582–601
- van Hoof A, Frischmeyer PA, Dietz HC & Parker R (2002) Exosome-mediated recognition and degradation of mRNAs lacking a termination codon. *Science* **295**: 2262–2264
- Vanacova S, Wolf J, Martin G, Blank D, Dettwiler S, Friedlein A, Langen H, Keith G & Keller W (2005) A new yeast poly(A) polymerase complex involved in RNA quality control. *PLoS Biol.* **3**: e189
- Vincent HA & Deutscher MP (2006) Substrate recognition and catalysis by the exoribonuclease RNase R. *J Biol Chem* **281**: 29769–29775
- Wasmuth EV & Lima CD (2012) Exo- and endoribonucleolytic activities of yeast cytoplasmic and nuclear RNA exosomes are dependent on the noncatalytic core and central channel. *Mol Cell* **48**: 133–144
- Wasmuth EV, Januszyk K & Lima CD (2014) Structure of an Rrp6-RNA exosome complex bound to poly(A) RNA. *Nature* **511**: 435–439
- Weir JR, Bonneau F, Hentschel J & Conti E (2010) Structural analysis reveals the characteristic features of Mtr4, a DEXH helicase involved in nuclear RNA processing and surveillance. *Proc Natl Acad Sci USA* **107**: 12139–12144
- Wyers F, Rougemaille M, Badis G, Rousselle J-C, Dufour M-E, Boulay J, Régnauld B, Devaux F, Namane A, Seraphin B, Libri D & Jacquier A (2005) Cryptic pol II transcripts are degraded by a nuclear quality control pathway involving a new poly(A) polymerase. *Cell* **121**: 725–737

Table I

X-ray data collection and refinement statistics

Figure legends

Figure 1

Direct interactions of the nuclear cofactors of the yeast exosome

(A) Schematic representation of the domain arrangement of the nuclear exosome cofactors from *S. cerevisiae* used in this study. Gray-filled rectangles denote domains whose structures are known from previous studies: the central region of Rrp6 with the exonuclease (Exo) and HRDC domains (Midgaard *et al*, 2006), the exosome-binding domain in the C-terminal region of Rrp6 (Makino *et al*, 2013a) and the entire helicase region of Mtr4 (Jackson *et al*, 2010; Weir *et al*, 2010). Colored rectangles highlight the N-terminal domains of Rrp6, Rrp47 and Mtr4 visualized in the structure of the ternary complex reported here. Truncation mutants engineered for the biochemical and structural analysis are indicated.

(B-G) Size-exclusion chromatography assay to assess formation of protein complexes. Purified samples (as indicated) were incubated and co-injected on an analytical size-exclusion column (Superdex 200 Increase 3.2/300, GE Healthcare, exclusion volume 0.8 ml). On the left are the overlays of the chromatograms (rel. AU and V_r denote relative absorbance and retention volume of the proteins, respectively). On the right, are the Coomassie-stained SDS-PAGE gels with samples from the corresponding peak fractions. The detailed analysis of the chromatography profiles is shown in Table E1.

Figure 2

Structure of the yeast Rrp6_N – Rrp47_N – Mtr4_N ternary complex

(A) Structure of the Rrp6_N – Rrp47_{ΔC} binary complex shown in cartoon representation with Rrp6 in red and Rrp47 in orange. The N- and C-terminal residues are indicated. This and all other cartoon drawings were generated with PyMOL (<http://www.pymol.org/>).

(B) Structure of the Rrp6_N – Rrp47_N – Mtr4_N ternary complex shown in cartoon representation in two orientations related by a 90° rotation about the horizontal axis. The orientation of the ternary complex in the left panel is the same as that of the binary complex in panel A. The secondary structure elements are labeled. A disordered region in the structure is indicated as a dotted line. The electron density for Mtr4_N (Fo-Fc, contoured at 2.0 σ in Pymol) and the model built into this density (blue) are shown.

(C) Superposition of the atomic models of Rrp6_N and Rrp47_N, showing the similarity of their secondary structure elements (labeled as in panel B).

(D) Topological diagram of the secondary structure elements of Rrp6_N and Rrp47_N. The left and right panels correspond to the views of the structure in the left and right panels of Fig 2B, respectively.

Figure 3

Rrp6_N and Rrp47_N form a highly intertwined structural module

(A) Intermolecular contacts between the α 1 and 2 helices (from both Rrp6_N and Rrp47_N), which form the center of the helical bundle. On the right is a zoom-in with a subset of the extensive Van der Waals interactions shown on the left.

(B) Intermolecular contacts between helices α 2 and α 3 (from both Rrp6_N and Rrp47_N), which are at the side of the bundle. A zoom in view of part of the interactions is shown on the right.

Figure 4

Structure-based sequence alignments of Rrp6_N, Rrp47_N and Mtr4_N

The alignments of Rrp6 (A), Rrp47 (B) and Mtr4 (C) include orthologues from the representative species *S. cerevisiae* (*S.c.*), *Neurospora crassa* (*N.c.*), *H. sapiens* (*H.s.*), *D. melanogaster* (*D.m.*) and *D. rerio* (*D.r.*), based on a comprehensive alignment. The secondary structure elements are shown above the sequences. Conserved residues are highlighted in color. Colored circles above the sequences identify residues involved in the interaction with Rrp6 (red circles), with Rrp47 (orange circles) and with Mtr4 (blue circles). Circles of two colors indicate residues involved in interactions with two partners in the ternary complex. Residues targeted for mutagenesis are highlighted with a black square.

Figure 5

Mtr4_N binds at an evolutionary conserved surface groove of Rrp6_N-Rrp47_N

(A) Surface representation of Rrp6_N – Rrp47_N colored according to sequence conservation (corresponding to the comprehensive alignments used for Fig 4). The complex is shown in two orientations related by a 180° rotation about the vertical axis. The concave surface of Rrp6_N – Rrp47_N is viewed on the left (with an orientation corresponding to that in Fig 2B, left panel) where Mtr4 is shown with the helix in cartoon representation. Peripheral patches of conserved residues of Rrp6 not involved in the interaction with Mtr4 are also indicated.

(B) Close-up view of the interactions of Mtr4_N with Rrp6_N and Rrp47_N. Interacting residues are shown in stick representation and labeled.

(C) Isothermal titration calorimetry experiments (ITC) of the Mtr4_N peptide with Rrp6 – Rrp47. The MicroCal cell was filled with Rrp6_N – Rrp47_{ΔC} complex at 50 μM and the Mtr4 peptide was injected at 500 μM concentration consecutively in 2 μl volumes. The left panel shows binding with the proteins used in the structure determination. Shown in the inset are the number of calculated binding sites (N), and the dissociation constant (K_d), as calculated with the program Origin. The middle and right panels show the corresponding ITC experiments with structure-based mutations. A Coomassie stained gel with the wild-type and mutant complexes used in these experiments is shown on the right.

Figure 6

Impact of Rrp6_N-Rrp47_N on ribonuclease activity

(A) Surface representation of Rrp6_N – Rrp47_N colored according to electrostatic potential (blue for electropositive and red for electronegative). Mtr4_N is shown in gray, with negatively charged residues in a stick representation. The molecule is viewed in the same orientations as in Fig 5A.

(B) Quantitative measurements of RNA-binding affinities in solution by fluorescence anisotropy using fluorescein-labeled homopolymeric substrates. The data were fitted to a binding equation describing a single-site binding model to obtain the dissociation constants (K_d). The best fit was plotted as a solid line. The K_d s and their corresponding errors are the mean and standard deviation of a minimum of 3 independent experiments and are compiled in the table (top panel).

(C) Nuclease activity of the indicated Rrp6 and Rrp6 – Rrp47 constructs towards single stranded RNAs and duplex RNAs with 3' overhangs. Substrates were designed to have a 17 base pair GC-rich duplex (ds17), corresponding to the 3' end of tRNA^{Tyr}

(Lorentzen *et al.*, 2008; Vincent & Deutscher, 2006), and a 3' overhang of 10 adenine nucleotides (A10). The RNAs were 5' end labeled with [$\gamma^{32}\text{P}$]ATP and the reaction products were resolved on 20% denaturing PAGE and visualized with a phosphorimager. A Coomassie stained gel with the wild-type and nuclease deficient mutant proteins used in the RNase activity and RNA affinity assays (B) is shown on the right.

Figure 7

Structure-based mutations in the Rrp6 N-terminal domain result in 5.8S RNA processing defects *in vivo*

(A) Northern blot analyses of RNA from *rrp6*, *mtr4-gfp* and *mtr4-gfp rrp6* double mutants. Strains were grown in selective minimal medium, unless indicated otherwise. Consecutive hybridizations of a single blot are shown; panels shown for lanes 1-6 and 7-11 are juxtaposed from a single image. The major RNAs detected by each probe are indicated on the right. Asterisks indicate truncated RNA fragments of U3, snR13 and 5S. The amount of “5.8S+30” RNA, the 5' ETS fragment and the major U3 and 5S degradation fragments in each mutant (indicated beneath the appropriate panel) is expressed relative to the *rrp47-zz* strain in lanes 1-6 and to the *mtr4-gfp* strain during growth in YPD in lanes 7-11.

(B) Spot growth assays of *rrp6* mutants. Serial dilutions of pre-cultures were spotted onto selective minimal medium plates and incubated at 30 °C or 37 °C. The plates were photographed after three days.

(C) Western analyses of *rrp6* mutants. (Upper panels) Expression levels of Rrp6 and the Rrp47-zz fusion protein in the *rrp6* mutants. (Lower panels) Mtr4-gfp fusion

protein expression levels in the *mtr4-gfp rrp6* double mutants. Pgk1 levels were analyzed as a loading control in each case.

Figure 8

Disruption of the Rrp6/Mtr4 interaction in yeast blocks growth of *mtr4-gfp* strains

(A) Plasmid shuffle assay on an *mtr4-gfp rrp6* Δ strain expressing zz-Rrp6. Transformants harboring *LEU2* plasmids encoding wild-type zz-Rrp6, the I14E, R18E variant or the vector alone were cultured in selective medium and then spotted onto medium lacking leucine or containing 5 FOA. Plates were incubated at 30 °C and photographed after three days.

(B) Pull-down assays of zz-Rrp6 with Mtr4-gfp. *Left Panels* Pull-downs of zz-Rrp6 in an *mtr4-gfp* strain harboring the vector (lane 1), expressing zz-tagged wild-type Rrp6 (lane 2) or the I14E,R18E variant (lane 3). The amount of Mtr4-gfp associated with Rrp6 is expressed relative to the negative control and is normalized to the Rrp6 levels in the eluates. The mean values of assays on two independent biological replicates are shown. Error bars indicate the experimentally observed range. *Right Panels* Pull-downs of zz-Rrp6 in a wild-type strain expressing the Mtr4-gfp fusion protein or the F7A,F10A mutant. A wild-type strain was transformed with plasmids expressing either non-tagged or zz-tagged Rrp6 and Mtr4-gfp or the F7A,F10A mutant and analyzed by western, as above.

(C) *mtr4* plasmid shuffle assay. An *mtr4* Δ mutant strain harboring a *URA3* plasmid containing the wild-type *MTR4* gene was transformed with *LEU2* plasmids encoding *mtr4-gfp*, *mtr4*_{F7,F10A} or *mtr4-gfp*_{F7A,F10A} mutants, the wild-type *MTR4* gene or the vector. Strains were grown up in selective medium and then spotted onto medium

lacking leucine (SD-Leu) or containing 5 FOA. The plates were incubated at 30°C and photographed after 3 days.

Figure 9

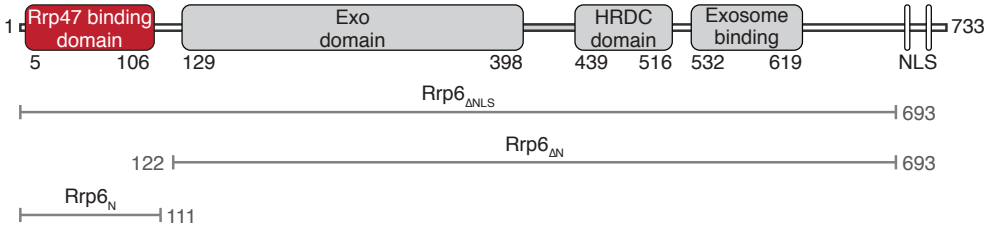
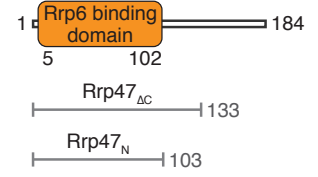
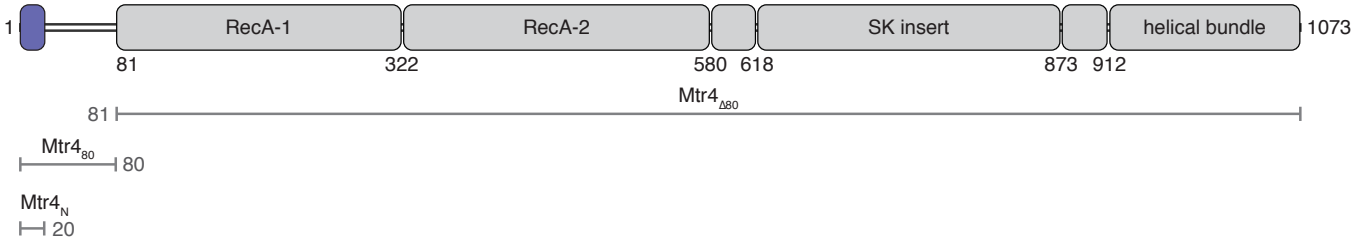
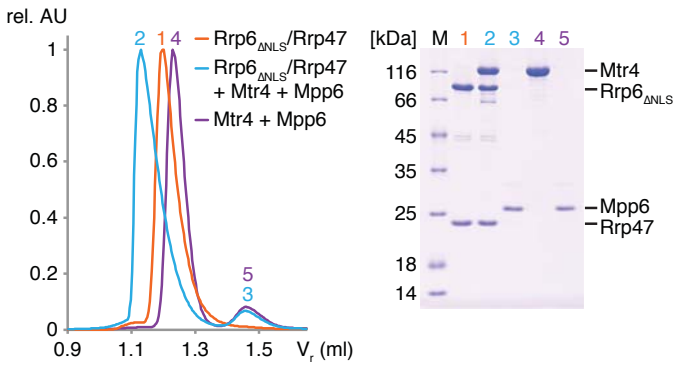
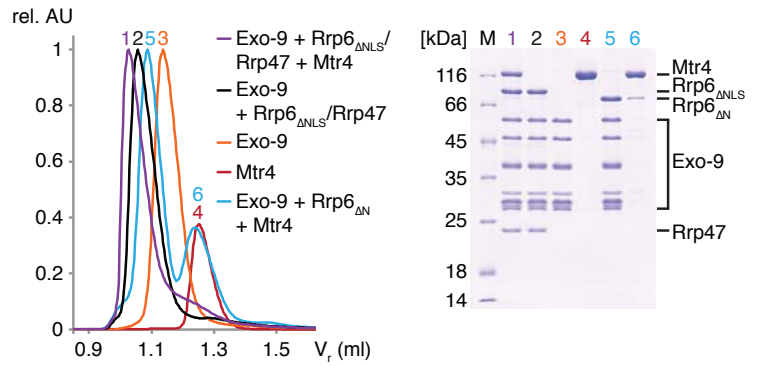
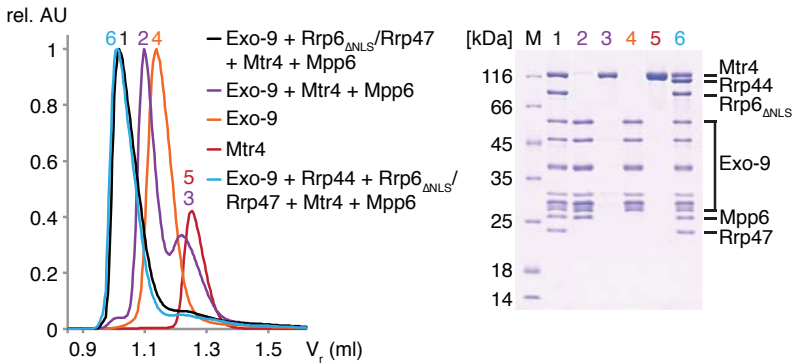
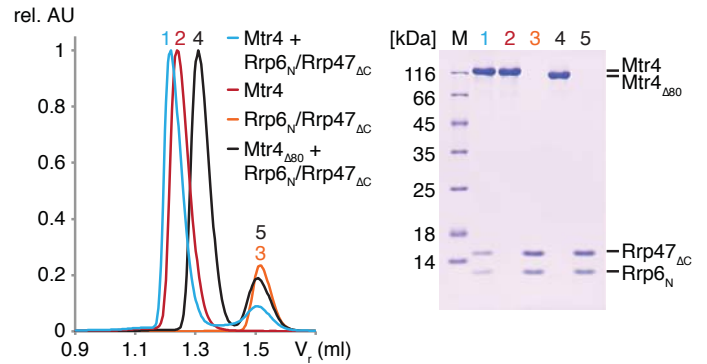
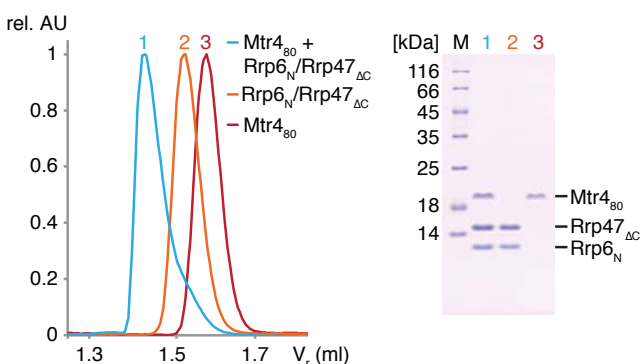
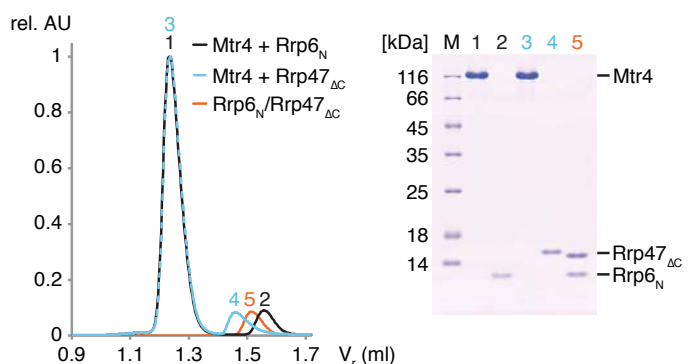
Model of the nuclear exosome complex

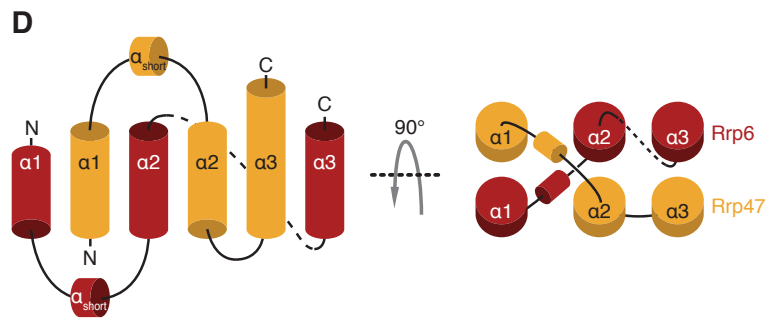
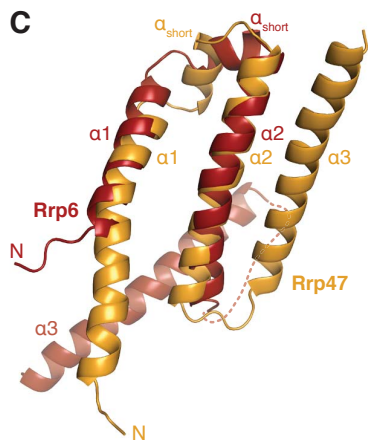
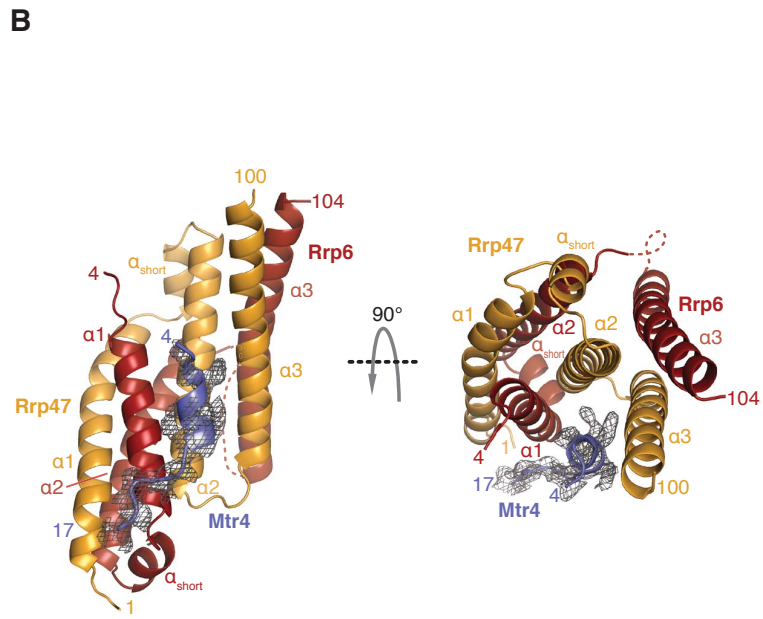
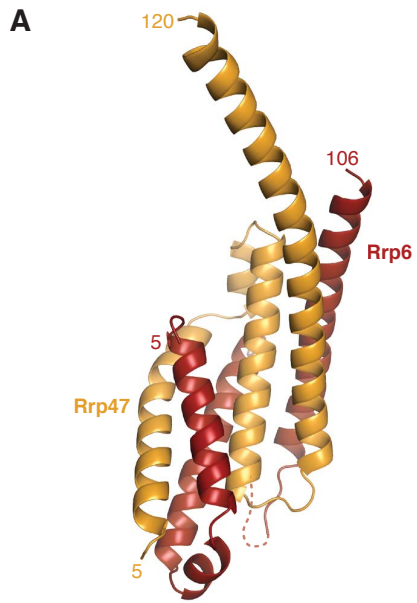
The schematic representation shows the architecture of the yeast nuclear exosome based on current structural and biochemical information. The exosome core (Exo-10) is depicted with the RNase PH-like subunits in gray, the S1/KH subunits in orange and Rrp44 in pink (based on the structure reported in Makino *et al*, 2013a). RNA is shown in black, threading through the internal channel and reaching the exoribonuclease site of Rrp44 (highlighted with a circle). The endonuclease site in the PIN domain of Rrp44 is also highlighted with a circle. Rrp6 is shown in red, with the exoribonuclease site highlighted as a circle. The exoribonuclease of Rrp6, depicted based on Midtgaard *et al*, 2006, is positioned near the exosome-binding domain of Rrp6, as determined by Makino *et al*, 2013a. Rrp47 is in gray while Mtr4 is in blue. The channel in the helicase core and the insertion domain of Mtr4 are indicated in the model (according to the structures reported by Jackson *et al*, 2010; Weir *et al*, 2010). The N-terminus of Mtr4 binds at the interface between Rrp6 and Rrp47. The N-terminal interaction regions of Rrp6, Rrp47 and Mtr4 are denoted by N. Mpp6 is shown tentatively at the top of Exo-10, as its binding is not dependent on Rrp44.

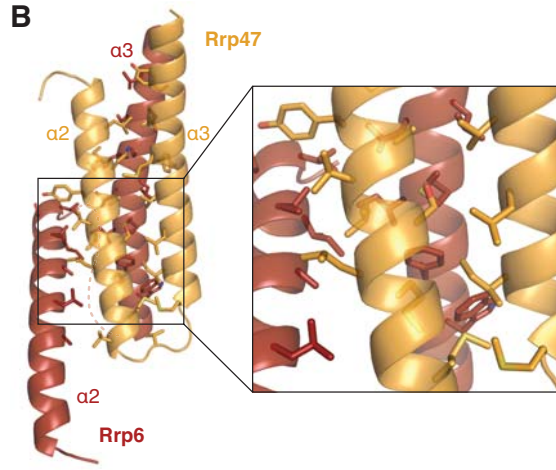
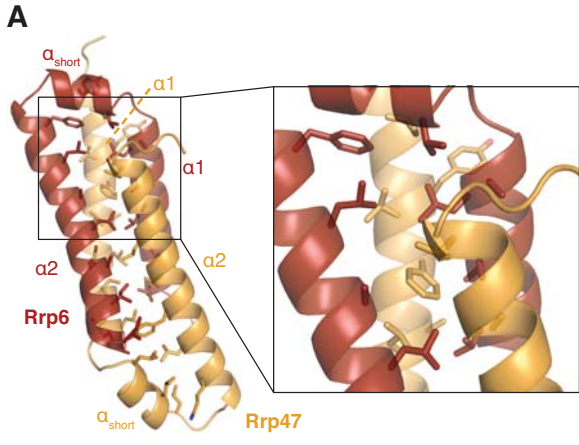
Table I. Crystallographic Statistics

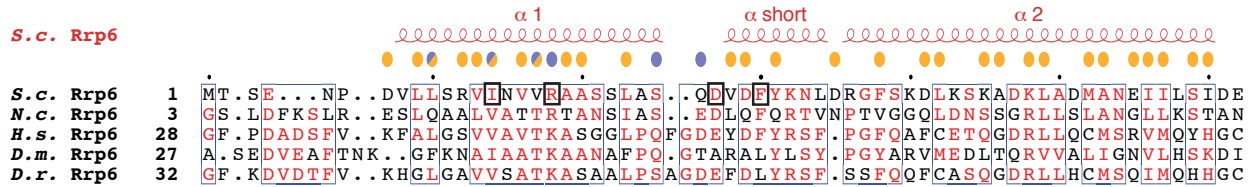
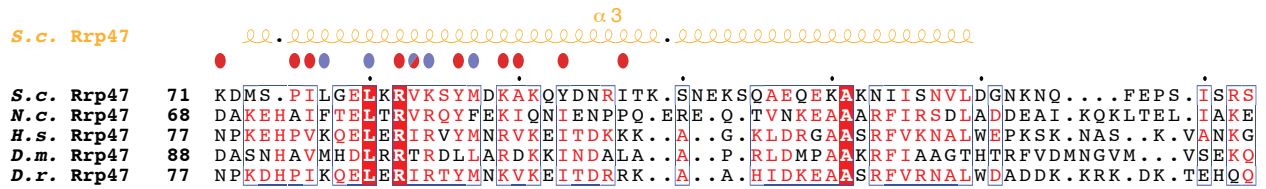
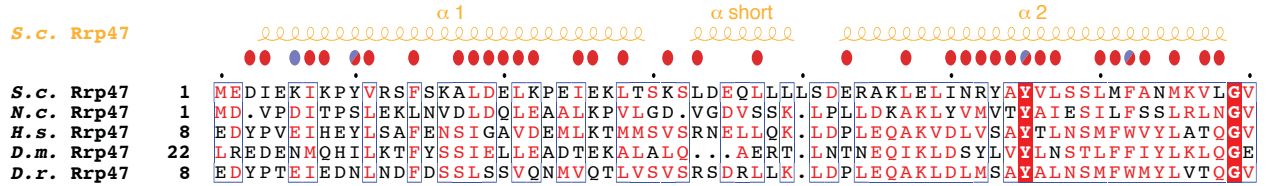
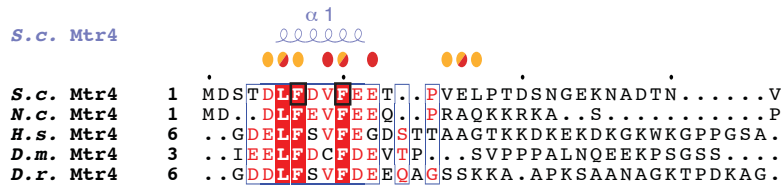
Data set	Rrp6 _N -Rrp47 _{ΔC} native	Rrp6 _N -Rrp47 _{ΔC} Ta ₆ Br ₁₄	Rrp6 _N -Rrp47 _{ΔC} Se-Met	Rrp6 _N -Rrp47 _N -Mtr4 _N native
Data collection				
Space group	P 41 2 2	P 41 2 2	P 41 2 2	P 3 1 2
Unit cell (a, b, c in Å)	98.5, 98.5, 208.0	98.6, 98.6, 205.3	97.9, 97.9, 207.7	142.7, 142.7, 63.5
Wavelength (Å)	0.873	1.255	0.979	1.000
Resolution range (Å)	69.62 – 2.64 (2.73 – 2.64)	88.85 – 5.19 (5.80 – 5.19)	48.96 – 3.59 (3.94 – 3.59)	47.42 – 2.40 (2.48 – 2.40)
Unique reflections	30965 (2987)	4311 (1169)	12424 (2850)	28898 (2781)
Completeness (%)	99.8 (98.4)	99.6 (98.6)	99.6 (98.5)	99.6 (96.3)
Multiplicity	10.5 (10.2)	11.7 (11.6)	41.8 (42.9)	17.3 (17.1)
Mean I / σ (I)	21.50 (2.94)	14.7 (3.5)	20.3 (8.6)	26.64 (1.68)
R-merge	0.098 (0.857)	0.140 (0.837)	0.278 (0.644)	0.092 (1.989)
CC1/2	0.999 (0.813)	0.998 (0.879)	0.998 (0.972)	1.000 (0.603)
Refinement				
R-work (%)	20.74			19.42
R-free (%)	23.81			23.86
Rmsd bonds (Å)	0.003			0.010
Rmsd angles (°)	0.62			1.40
Average B-factor	60.30			71.7
Ramachandran favored (%)	99			99
Ramachandran outliers (%)	0.18			0.36

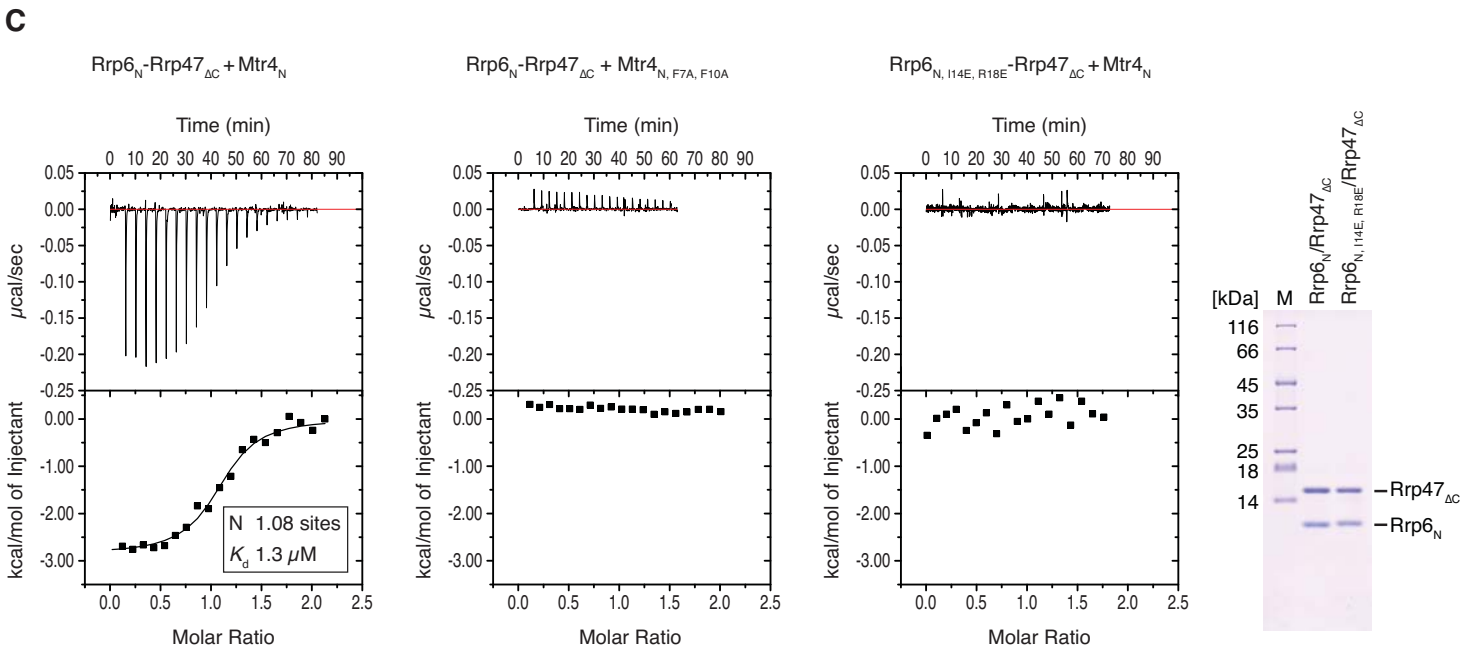
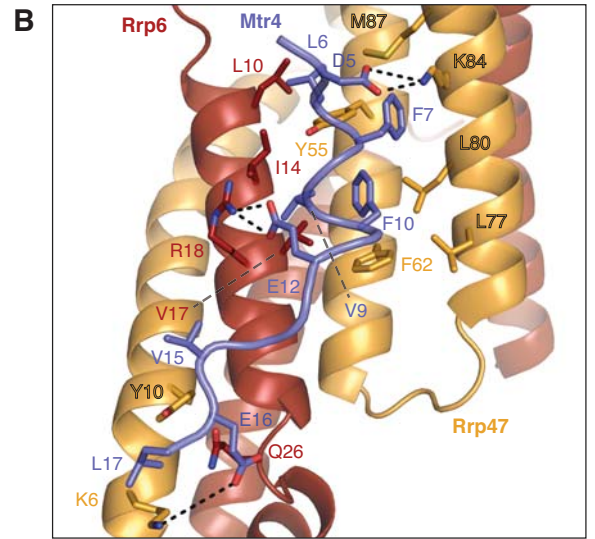
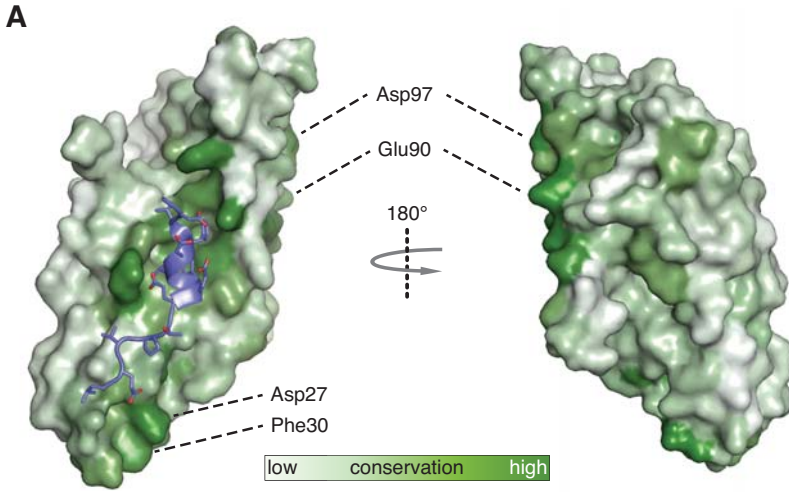
Values in parentheses correspond to the highest-resolution shell.

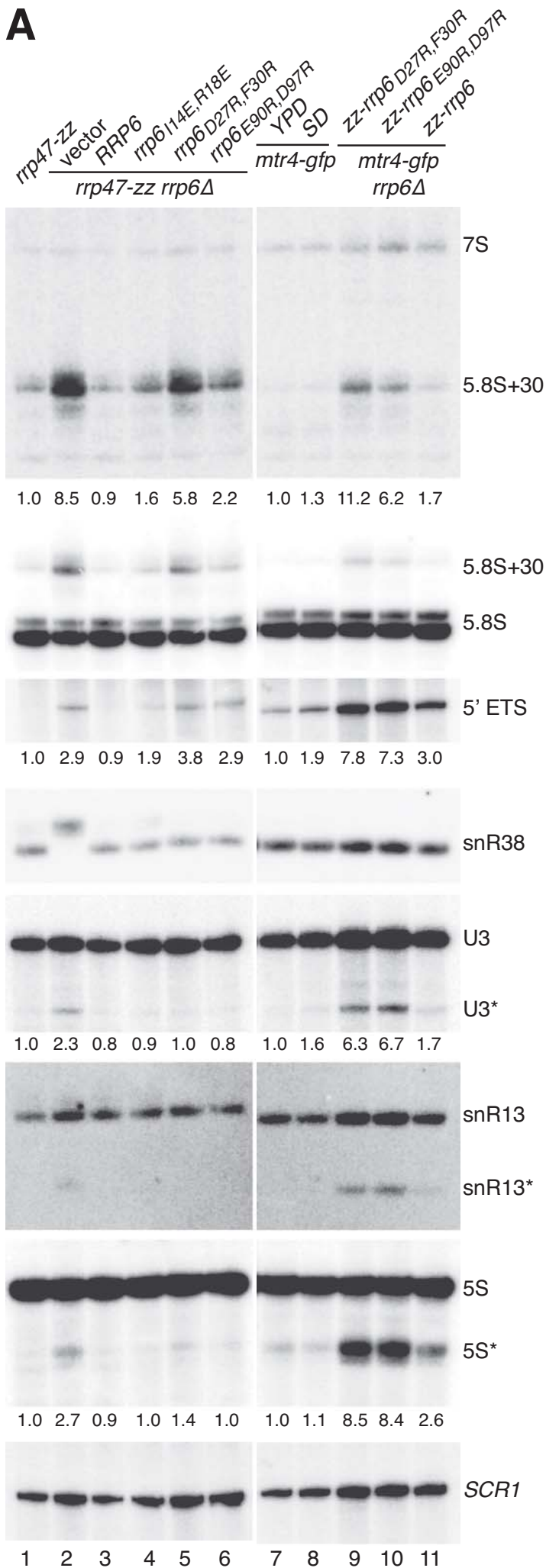
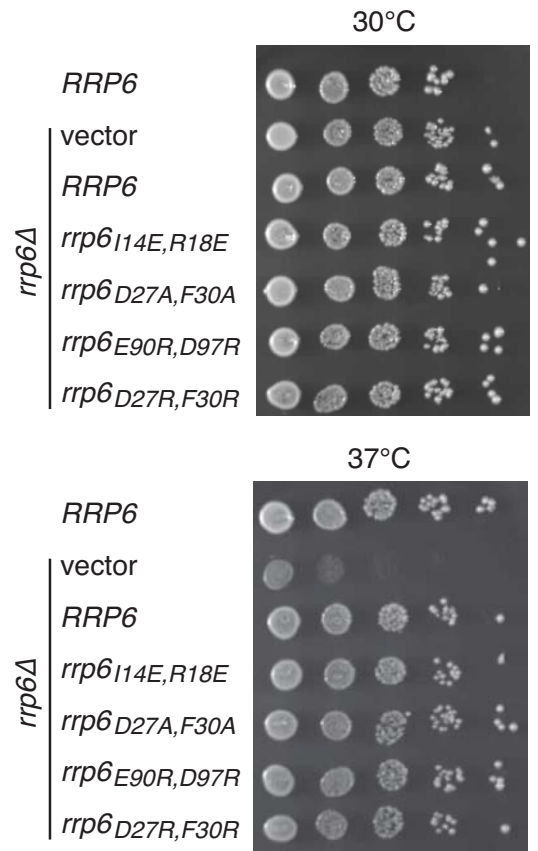
A**Rrp6****Rrp47****Mtr4****B****C****D****E****F****G**





A**B****C**



A**B****C**